Kushal Purbia

MMT31

VVR

Document Details

Submission ID
trn:oid:::27535:141245979

Submission Date
Jun 1, 2026, 2:37 PM GMT+5:30

Download Date
Jun 9, 2026, 5:55 PM GMT+5:30

File Name
MMT31.docx

File Size
12.0 MB

65 Pages

11,113 Words

62,146 Characters

7% Overall Similarity

The combined total of all matches, including overlapping sources, for each database.

Filtered from the Report

- Bibliography
- Small Matches (less than 14 words)

Exclusions

- 19 Excluded Matches

Match Groups

30 Not Cited or Quoted 6%
Matches with neither in-text citation nor quotation marks

0 Missing Quotations 0%
Matches that are still very similar to source material

5 Missing Citation 1%
Matches that have quotation marks, but no in-text citation

0 Cited and Quoted 0%
Matches with in-text citation present, but no quotation marks

Top Sources

5% Internet sources
5% Publications
4% Submitted works (Student Papers)

Match Groups

- **30** Not Cited or Quoted 6%
  Matches with neither in-text citation nor quotation marks
- **0** Missing Quotations 0%
  Matches that are still very similar to source material
- **5** Missing Citation 1%
  Matches that have quotation marks, but no in-text citation
- **0** Cited and Quoted 0%
  Matches with in-text citation present, but no quotation marks

Top Sources

5% Internet sources
5% Publications
4% Submitted works (Student Papers)

Top Sources

The sources with the highest number of matches within the submission. Overlapping sources will not be displayed.

1	Internet	power.kaist.ac.kr <1%
2	Internet	ajitelectricals.com <1%
3	Student papers	TechKnowledge on 2015-12-03 <1%
4	Publication	Behnam Koushki, Praveen Jain, Alireza Bakhshai. "A single-stage bi-directional AC... <1%
5	Internet	www.dspace.dtu.ac.in:8080 <1%
6	Internet	scholar.archive.org <1%
7	Publication	Zhiqiang Guo, Zhijie Huang, Zhongyuan Chen, Xiaoyong Sun. "Multi-Objective Opt... <1%
8	Internet	www.proceedings.com <1%
9	Internet	dspace.dtu.ac.in:8080 <1%
10	Internet	patents.justia.com <1%

11 Internet

www.grafiati.com <1%

12 Student papers

Midlands State University on 2025-10-24 <1%

13 Student papers

Universiti Tenaga Nasional on 2015-10-04 <1%

14 Publication

Xiaojun Xu, , Wei Liu, and A.Q. Huang. "Two-Phase Interleaved Critical Mode PFC ... <1%

15 Publication

Yue Chen, Xinke Wu, Zhaoming Qian, Wenping Zhang. "Design and optimization o... <1%

16 Publication

Kushank Singh, Vanjari Venkata Ramana. "Design and Analysis of Vienna Rectifier... <1%

17 Internet

pure.bit.edu.cn <1%

18 Student papers

University of Nottingham on 2024-09-02 <1%

19 Internet

macau.uni-kiel.de <1%

20 Internet

www.peeref.com <1%

21 Publication

Radko Stoyanov, Orlin Stanchev, Vencislav Valchev, Angel Marinov. "Optimising s... <1%

22 Internet

dspace.daffodilvarsity.edu.bd:8080 <1%

23 Student papers

Brunel University on 2026-02-28 <1%

24 Student papers

TUS Technological University of the Shannon: Midwest, Moylish Campus on 2026-... <1%

25 Student papers

University College London on 2020-08-11 <1%

26 Student papers

Visvesvaraya National Institute of Technology on 2026-05-20 <1%

27 Internet

web.uri.edu <1%

28 Publication

Wajahat Khan, Jahangeer Ahmad Dar, Karthik Singh Parihar, Mukesh Kumar Path... <1%

29 Internet

www.mdpi.com <1%

30 Student papers

AUT University on 2024-10-18 <1%

31 Student papers

Queen's University of Belfast on 2021-04-21 <1%

32 Student papers

University College London on 2021-08-31 <1%

M.Tech (Power Electronics and Systems)

Design and Implementation of Power Converters for Charging Applications with Improved PFC

A PROJECT REPORT
SUBMITTED IN PARTIAL FULFILLMENT OF THE REQUIREMENTS FOR THE AWARD OF THE DEGREE OF

MASTER OF TECHNOLOGY

in

Power Electronics & Systems

Submitted by:

2K24/PES/13

KUSHAL PURBIA

Under the supervision of

DR. VANJARI VENKATA RAMANA
(Assistant Professor, EED, DTU)

Department of Electrical Engineering

DELHI TECHNOLOGICAL UNIVERSITY
(Formerly Delhi College of Engineering) Bawana Road, Delhi-110042

MAY, 2026

Kushal Purbia 2026

DELHI TECHNOLOGICAL UNIVERSITY

(Formerly Delhi College of Engineering)
Bawana Road, Delhi - 110042

CANDIDATE DECLARATION

I, Kushal Purbia (2K24/PES/13) of M. Tech. (POWER ELECTRONICS & SYSTEMS), hereby declare that the project report titled "**Design and Implementation of Power Converters for Charging Applications with Improved PFC**" which is submitted by me to the Department of Electrical Engineering, Delhi Technological University, Delhi in partial fulfilment of the requirement for the award of the degree of Bachelor of Technology, is original and not copied from any source without proper citation. This work has not previously formed the basis for the award of any Degree, Diploma Associateship, Fellowship or other similar title or recognition.

Place: Delhi
Date: 31/05/2026

Kushal Purbia

DELHI TECHNOLOGICAL UNIVERSITY

(Formerly Delhi College of Engineering)
Bawana Road, Delhi - 110042

CERTIFICATE

This is to certify that the dissertation entitled **Design and Implementation of Power Converters for Charging Applications with Improved PFC** submitted by KUSHAL PURBIA (Roll No. 2K24/PES/13) in partial fulfillment of the requirements for the award of the degree of Master of Technology in POWER ELECTRONICS & SYSTEMS, at Delhi Technological University, is a record of bonafide work carried out by him under my supervision and guidance.

The work embodied in this dissertation has not been submitted to any other University or Institute for the award of any degree or diploma to the best of my knowledge.

Place: Delhi
Date: 31/05/2026

Dr. Vanjari Venkata Ramana
(SUPERVISOR)

ACKNOWLEDGEMENT

I would like to express my gratitude towards all the people who have contributed their precious time and effort to help me without whom it would not have been possible for me to understand and complete the project.

I would like to thank **Dr. Vanjari Venkata Ramana** (Assistant Professor, Department of Electrical Engineering, DTU, Delhi) my Project guide, for supporting, motivating and encouraging me throughout the period of this work was carried out. His readiness for consultation at all times, his educative comments, his concern and assistance even with practical things have been invaluable. I would also like to thank the Centre of Excellence for Electric Vehicles and Related Technologies, Delhi Technological University for providing necessary facilities for performing my research work.

Finally, I must express my very profound gratitude to my parents, seniors and to my friends for providing me with unfailing support and continuous encouragement throughout the research work.

Date: 31/05/2026

Kushal Purbia
M. Tech (Power Electronics & Systems)
2K24/PES/13

ABSTRACT

With increasing popularity of electric vehicles and the growing need for fast and efficient charging stations, there exists a necessity for designing a power converter system that will provide a highly regulated DC output voltage at low voltage levels in response to a standard AC supply voltage. In this thesis, a two-stage power converter system consisting of an interleaved boost power factor correction converter, which is followed by a full-bridge LLC resonant converter, will be designed and analyzed. The proposed power converter system has been designed for a rated power of 3 kW, which provides a highly regulated output voltage of 48 V.

For providing high efficiency and reduced switching losses, the first stage consists of an interleaved boost power factor correction converter, which directly converts the mains AC voltage (230 V) to regulated DC link voltage of 400 V. This stage ensures regulation of the DC link voltage to 400 V and provides a high-power factor due to shaping of input current waveforms to follow the input sinusoidal voltages. Interleaving is done by means of 180^0 out-of-phase gating signals applied to two identical boost converters operated in parallel with one another.

The second stage consists of a full-bridge LLC resonant converter that accepts the 400 V regulated DC link voltage and delivers a controlled output voltage of 48 V at 3 kW. The operating principles of the LLC converter are examined across three frequency regions: at resonance, below resonance, and above resonance.

The first harmonic approximation method is employed to derive the voltage gain expression, which forms the basis of a systematic resonant tank design procedure covering the selection of Q_{max}, optimization of the inductance ratio m, and explicit calculation of the resonant component values L_r, C_r, and L_m. A closed-loop voltage controller based on pulse frequency modulation is designed to regulate the 48 V output under both load-side and input-side disturbance conditions.

The complete system is modelled and validated through simulation studies in MATLAB-Simulink. Results confirm stable output voltage regulation at 48 V, high power factor at the AC input, satisfactory dynamic response under load and input voltage variations, and maintained soft-switching operation across the intended operating range of the full-bridge LLC resonant converter.

TABLE OF CONTENT

LIST OF FIGURES

LIST OF TABLES

LIST OF ABBREVIATION

EV	Electric Vehicle
PF	Power Factor
THD	Total Harmonic Distortion
PFC	Power Factor Correction
DBR	Diode Bridge Rectifier
PI	Proportional Integral

PID	Proportional Integral Derivative
FFT	Fast Fourier Transform
CCM	Continuous Conduction Mode
CRM	Critical Conduction Mode
PWM	Pulse width Modulation
AC	Alternating Current
PHEV	Plug in Hybrid Electric Vehicle
DC	Direct Current
LLC	Inductor-Inductor-Capacitor
PFM	Pulse Frequency Modulation
VOLT	Voltage
FHA	First Harmonics Approximation
DSP	Digital Signal Processor
MOSFET	Metal Oxide Semiconductor Field Effect Transistor
ZVS	Zero Voltage Switching
ZCS	Zero Current Switching
PI	Proportional Integrator
DSO	Digital Signal Oscilloscope
RMS	Root Mean Square
AMPS	Ampere
kHz	Kilohertz
KW	Kilowatt

LIST OF SYMBOLS

S_1, S_2, Q_1 ,Q_2, Q_3, Q_4	MOSFET Switches
V_o	Output Voltage
$V_{d(t)}$	Output Voltage of DBR
i_{L1},i_{L2}	Current through both Inductors
i_C	Current through Capacitor
i_o	Output Current
V_{DC}	DC Link Voltage

I_{in}	Input Current
D_1, D_2, D_3, D_4, D_5, D_6	DIODE
F_{SW}	Switching Frequency
P_o	Output Power
I_r	Resonant Current
I_m	Magnetizing Current
I_d	Diode Current

CHAPTER 1
INTRODUCTION

1.1 BACKGROUND

With the rapid growth of renewable energy, electric vehicles, and portable electronic devices, the demand for effective battery charging solutions has risen significantly. Traditional battery chargers often have poor power factor, high harmonic distortion, and limited efficiency. These issues can negatively impact both the power grid and the battery's lifespan. To address these problems, modern charger designs use improved converter layouts and control methods. These ensure high efficiency, lower power losses, and compliance with international power quality standards [1].

Power factor correction is a fundamental requirement in modern AC-DC power conversion systems and aims to shape the input current waveform to be in phase with the mains voltage to maximize the real power taken from the supply. In an ideal power factor correction circuit, the converter operates as a purely resistive load for its AC input terminals, drawing a sinusoidal current with no harmonic distortion and in phase with the supply voltage, with a unity power factor, and according to international standards for harmonic emissions such as the IEC 61000-3-2 [2, 3].

Resonant circuits have been widely adopted in power conversion systems for their ability to reduce switching losses and suppress electromagnetic interference. Among the various resonant topologies, the LLC resonant converter has emerged as a preferred solution for isolated DC-DC conversion owing to its high efficiency, low EMI, and compact power density. The designation LLC is derived from the three principal passive elements involved in the resonant mechanism the leakage inductance L_r and magnetizing inductance L_m of the high-frequency transformer, along with the resonant capacitor C_r. A distinctive feature of the LLC topology is the presence of two resonant frequencies: the series resonant frequency f_r established by L_r and C_r, and a lower resonant frequency f_m determined by the combined inductance ($L_r + L_m$) and C_r, which allows the converter to maintain soft-

switching across a wider range of operating conditions compared to single-resonant topologies [4, 5].

The full-bridge LLC resonant converter has attracted a great deal of interest in high-performance power conversion applications due to its inherent merits of high conversion efficiency, reduced electromagnetic interference, and compact power density. The design of an LLC resonant converter, however, is much more complex than the design of conventional pulse width modulated converters and requires careful selection of resonant tank parameters and an iterative procedure to meet multiple design constraints simultaneously. The traditional design methodologies rely heavily on graphical gain curves and calculus-based derivations that, although mathematically valid, tend to be time-consuming and challenging to extend to various operating specifications [5,6].

1.2 LITERATURE REVIEW

There has been a rapid evolution in the development of AC/DC power conversion products for charging applications. Numerous advances in using more energy-efficient and grid-friendly forms of DC chargers for charging peripherals (such as batteries) has resulted in the evolution of these converters over time. Early AC/DC converters were typically designed to regulate their output to supply a constant DC output but had little regard to the quality of the input current. However, with the emergence of non-linear loads and electric vehicle charging systems, the problem of poor power factor and harmonics has become more prevalent [1].

24

Many researchers have begun to study design approaches to create power factor correction (PFC) circuits to shape the input current waveform to more closely follow the input voltage waveform so that the overall power quality is improved. There have been several research papers published demonstrating the importance of using PFC circuits.

For the past two decades, research has been predominantly on LLC resonant converter; the early foundational work was made by in [7], who presented the detailed analysis and design approach for LLC resonant converter which served as theoretical background for most of the further works. It also demonstrated a methodology for analyzing voltage gain characteristics and behaviour of resonant tank. In [8], the authors also proposed an optimum design method which dealt with the repetitive procedure in designing resonant tank parameters. The conflict

between inductance ratio, quality factor and attainable range of voltage gain has been pointed out in this initial research and still one of main issues to be considered in current research.

The development of electrical vehicle technology drew many attentions to design dedicated to battery charger. The authors in [9] presented the design methodology of LLC resonant converter for electric vehicle battery charger which takes into account of the wide output voltage ranges required in constant current and constant voltage operation. Li, Deng and Mi [10] showed a single-stage resonant battery charger with intrinsically achieved power factor correction which eliminates the necessity of a PFC circuit, reducing the number of components and improving the efficiency of the entire system; However, the design of the single stage topology becomes much more complicated in resonant tank parameters.

For applications with higher input voltage range, Lee and Moon [8] discussed a three level LLC series resonant converter which allows wider and higher input voltage ranges. Three level resonant structure significantly reduces the voltage stress on the resonant tank components. Hence, it has some advantage for application under higher voltage condition which are not possible to apply standard half-bridge or full-bridge configuration due to the stress on the components.

Another common issue related with LLC converter is low efficiency and regulation performance under light-load conditions. Kim et al. [11] addressed load adaptive phase shift control in full bridge LLC resonant converter; modification of control pattern at light-load condition indeed results in a dramatic efficiency improvement over standard frequency-only modulation. In [12], the authors proposed to tackle this issue with impedance analysis; a through investigation of converter impedance characteristics at different load conditions is presented to find the optimal control strategy. Their analysis further verified that the light-load performance of LLC converter can't solely be achieved through frequency modulation only.

S. No.	Title	Authors	Year	Key Contribution
1	Interleaved Critical Current Mode Boost PFC Converter With	Yang Yang, and Zhihong Ye	2011	Studies CRM interleaved boost PFC using a coupled inductor to reduce ripple,

	Coupled Inductor [13]			improve efficiency, and shrink magnetic size.
2	Two-Phase Interleaved Critical Mode PFC Boost Converter With Closed Loop Interleaving Strategy [14]	Xiaojun Xu, Wei Liu, and Alex Q. Huang,	2009	Proposes a closed-loop interleaving control ensuring precise 180° phase shift and current balancing.
3	Performance Evaluation of Bridgeless PFC Boost Rectifiers [15]	Laszlo Huber; Yungtaek Jang; Milan M. Jovanovic	2008	Compares several bridgeless boost PFC rectifiers, showing improved efficiency and lower conduction losses versus conventional boost PFC.
4	Extended Range Bridgeless PFC Converter With High-Voltage DC Bus and Small Inductor [10]	Hamed Valipour; Mohammad Mahdavi; Martin Ordonez	2021	Proposes a bridgeless PFC converter that supports a very wide AC input range while keeping high efficiency and reduced inductor size.
5	A High-Performance Single-Phase AC-DC Power Factor Corrected Boost	Fariborz Musavi; Wilson Eberle; William G. Dunford	2010	Designs a boost PFC front-end specifically for PHEV battery chargers with high

	Converter for plug in Hybrid Electric Vehicle Battery Chargers [17]			efficiency and near-unity power factor.
6	Single-Stage Resonant Battery Charger With Inherent Power Factor Correction for Electric Vehicles [18]	Siqi Li; Junjun Deng; Chunting Chris Mi	2013	
7	Multi-objective Genetic Algorithm Based Optimal Design Methodology for LLC Resonant Converter [19]	M. F. Menke and S. L. Avila	2022	Presented a systematic design methodology for LLC resonant converters considering resonant tank parameters, voltage gain characteristics, and soft-switching operation.
8	Analysis and Design of a Three-Level LLC Series Resonant Converter for High- and Wide-Input-Voltage Applications [8]	Il-Oun Lee, and Gun-Woo Moon		Introduced a three-level LLC resonant converter suitable for wide-input-voltage applications with reduced voltage stress and improved efficiency.
9	Analysis on Load-Adaptive Phase-	Jae-Hyun Kim, Dong-Wook	2016	Developed a load-adaptive phase-shift

	Shift Control for High-Efficiency Full-Bridge LLC Resonant Converter under Light-Load Conditions [11]	Kim, Gun-Woo Moon		control strategy to improve light-load efficiency in full-bridge LLC resonant converters.
10	Analysis on Synchronous Rectifier Control to Improve Regulation Capability of High-Frequency LLC Resonant Converter [20]	Min-Jae Kim, Gun-Woo Moon	2018	Investigated synchronous rectifier control methods for improving voltage regulation and efficiency in high-frequency LLC resonant converters.
11	High-Efficiency LLC Resonant Converter With High Voltage Gain Using an Auxiliary LC Resonant Circuit [21]	Dong-Kwan Kim , Cheol-O Yeon , Jae-Hyun Kim , Yeonho Jeong , and Gun-Woo Moon	2015	Proposed an LLC converter topology with auxiliary LC resonant circuitry to achieve high voltage gain and improved conversion efficiency.
12	Improving the Light-Load Regulation Capability of LLC Series Resonant Converter Using	Younghoon Cho, Gun-Woo Moon	2016	Presented an impedance-analysis-based control approach to enhance light-load regulation performance of

	Impedance Analysis [12]			LLC resonant converters.
13	A Novel Accurate Primary-Side Control Method for Half-Bridge LLC Resonant Converter [22]	Jae-Bum Lee, Chong-Eun Kim, Jae-Hyun Kim, Cheol-O Yeon, Young-Do Kim, and Gun-Woo Moon	2014	Proposed a primary-side control technique eliminating the need for opto-couplers while maintaining accurate output voltage regulation
14	Design and Analysis of LLC Resonant Converter for Electric Vehicle Battery Charging [9]	Shreyas, Mayank Kumar	2023	The paper presents an LLC resonant converter for use in electric vehicle (EV) battery charging applications. The resonant converter is the most efficient and has a soft-switching capability.
15	Resonant LLC converter for E-bike charger [23]	Rahul Pandey and Bhim Singh	2019	The LLC resonant converter is proposed for use in E-bikes with high efficiency and decreased losses due to switching operations. The implementation of Zero Voltage Switching (ZVS) provided soft-switching operations, enhancing the

				reliability and thermal performance of the converter. High frequency operations considered when selecting the topology will allow for smaller converters and greater power density, making the topology appropriate for the compact design of E-bike charging system

1.3 Research Gap

While PFC converters and LLC resonant converters have been individually studied in great depth, their combined two-stage integration where an interleaved boost PFC feeds directly into a full-bridge LLC stage has not been thoroughly investigated from a co-design perspective. Most studies treat the two stages independently, without addressing how front-end voltage ripple from the PFC stage affects the dynamic behaviour and control stability of the downstream LLC converter.

A significant portion of existing literature on LLC resonant converters focuses on half-bridge configurations, and comparatively less work has been reported on full-bridge LLC topologies specifically designed for high-power battery charging applications in the 3-kW range. Most published designs either target low-power consumer electronics or server power supplies, leaving a gap in systematic design procedures tailored for electric vehicle on-board charging at 48 V output.

Control of the LLC resonant converter under wide input voltage variation remains an open area. Many existing control strategies are validated only for a fixed DC bus voltage, and their performance under realistic input disturbances introduced by the PFC stage is rarely demonstrated. This gap is particularly relevant for EV

charging scenarios where mains voltage fluctuations directly propagate through the system.

The design optimization of the resonant tank specifically the simultaneous tuning of the quality factor Q and inductance ratio m has largely relied on graphical methods and manual iteration, which are time-consuming and not easily reproducible. A clear, step-by-step analytical design methodology that removes dependence on visual gain plots and reduces iteration cycles is still lacking in most published works.

Lastly, most simulation-based validations in the literature cover only steady-state performance, with limited attention given to transient response under step load changes and input voltage disturbances together. A comprehensive validation covering both disturbance types simultaneously, particularly for a two-stage PFC-LLC system, has not been widely reported.

1.4 Research Objectives

The main aim of this work is to design and implement an efficient two-stage power conversion system for lithium-ion battery charging in electric vehicle applications.

1) To design the interleaved boost power factor correction stage that interfaces directly with the 230 V AC mains supply, shapes the input current to follow the sinusoidal supply voltage waveform, and regulates the DC link voltage to 400 V while achieving high power factor and low total harmonic distortion at the AC input.
2) To develop a full-bridge LLC resonant converter across its three frequency operating regions at resonance, below resonance, and above resonance and identify the conditions necessary to achieve zero voltage switching on primary side switches and zero current switching on secondary side diodes throughout the intended operating range for the specified 3 kW, 48 V output rating.
3) To design a closed-loop voltage controller based on pulse frequency modulation for the LLC converter stage, capable of maintaining stable 48

V output regulation under both load side disturbances and input side voltage variations introduced from the front-end PFC stage.

4) To validate the complete two-stage interleaved boost PFC and full-bridge LLC resonant converter system through comprehensive simulation studies in MATLAB-Simulink, verifying steady state performance, transient response under step load changes, and dynamic behaviour under input voltage perturbations across the full operating range.

1.5 REPORT ORGANIZATION

- **Chapter 1 – Introduction:** Presents the motivation, objectives, background, literature review and scope of the work along with a brief overview of the proposed Interleaved Boost PFC and Full Bridge Resonant LLC converter.
- **Chapter 2 – Design and Analysis of Interleaved Boost PFC Converter:** Outlines the Design Methodology for the Proposed PFC Converter including Small Signal Modelling, Component Selection, and Theoretical Analysis and Simulation Results
- **Chapter 3 – Design and Analysis of Full Bridge LLC Resonant Converter:** Description of the Design Approach for the Proposed LLC Resonant Converter (Includes Design Process, Selection of Components, and Theoretical Analyses & Simulations)
- **Chapter 4 - Two Stage Interleaved Boost PFC Fed Full Bridge LLC Resonant Converter:** Outlines the Design Methodology for the Proposed Cascaded LLC Network (Includes Methodology for Cascaded Design of PFC Fed LLC Network, Parameter Table, Theoretical Analysis/Simulation Results)
- **Chapter 5 – Hardware Implementation:** A prototype of dc to dc interleaved boost converter is done & obtained results are shown.
- **Chapter 6 – Conclusion and Future Work:** Summarizes the key findings of the project and suggests possible directions for further research and improvements.

CHAPTER 2

DESIGN AND ANALYSIS OF INTERLEAVED BOOST PFC CONVERTER

2.1 INTRODUCTION

The requirement for power factor correction (PFC) has become an important part of modern power electronics to achieve energy efficiency and satisfy international standards (e.g., IEC 61000-3-2). Conventional single-phase Boost PFC converters are widely used because they provide the capability to shape the input current, achieve a near unity power factor, and regulate the DC-bus voltage. However, as the power levels increase, single Boost PFC converters cannot sustain their operation due to increasing current stress and losses and poor thermal performance. This results in decreased efficiency and reliability for the entire system. An alternative solution is the interleaved Boost PFC converter, which operates with two or more Boost converter phases running in parallel. The switching signals from each phase are dispersed in time (achieved using a phase shift), thus reducing both the input and output current ripple and ensuring that heat is dissipated uniformly among multiple components. This allows the interleaved Boost PFC converter to be an effective solution to the challenges of PFC for medium to high-power applications, including electric vehicle charging systems, renewable energy systems and power supplies for industrial applications [1].

The interleaved Boost PFC will require to have an efficient control strategy in order to have stable operation. This paper describes the implementation of a Dual-Loop PID Controller which consists of a current Control (inner loop) and Output Voltage Control (outer loop). The current Control works by making sure the input current tracks a sinusoidal reference waveform derived from the input voltage; thus achieving effective PFC. The Outer Loop regulates the DC bus Voltage to a constant Value while providing varying loads PFC and also maintaining a Constant bus voltage with different loads and disturbances input. Due to their simplicity, robustness, reliability, and also ability to respond quickly to dynamic changes in an application's environment, PID controllers make them ideal for use in Real-time Applications. This section covers the concept of an Interleaved Boost PFC

Converter utilizing Dual-Loop PID control, as well as the advantages claimed for using Dual-Loop PID control above traditional PFC methods. The following chapters will cover the design of the proposed system, the modeling of the controller, the simulation analysis performed on the controller, and an assessment of the performance using the proposed methodology.

2.2 Circuit Diagram

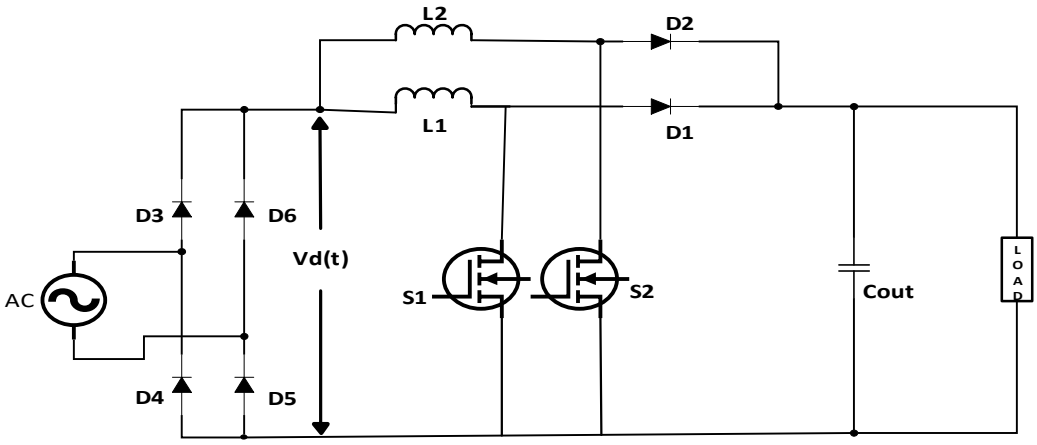

Fig 2.1. Two Phase Interleaved Boost PFC Converter.

IBC consists of two switches, which makes it possible to work in four modes during a given duty cycle. The operating states of the converter are:

2.3 Switching Pulses

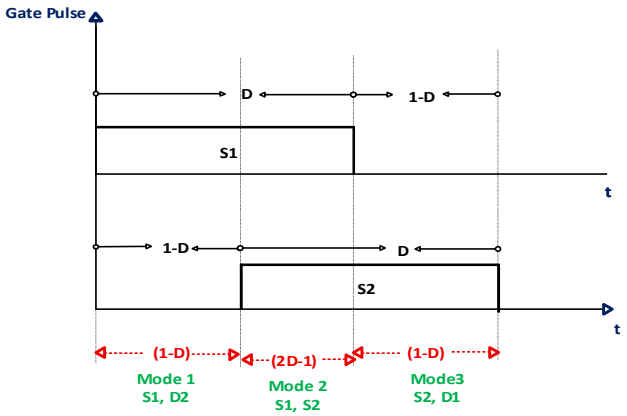

Fig: 2.2 Gate Pulses for Duty>0.5.

- **Mode 1: Switch 1 ON, Switch 2 OFF:**

In this mode, the input voltage source is connected to the inductor by turning on switch 1. The magnetic field stores energy as the inductor current increases. The Switch 2, is still off.

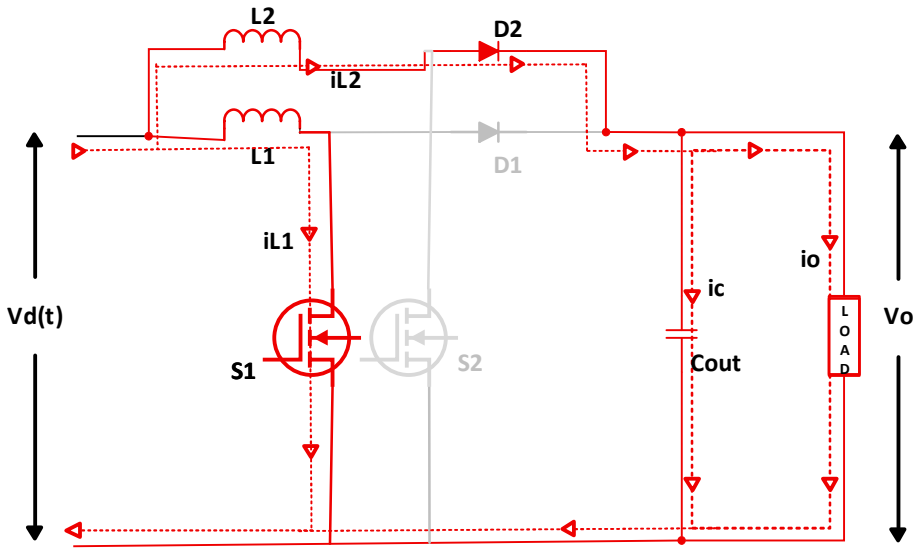

Fig 2.3 Mode 1(S1 & D2 ON).

- **Mode 2 - Both switches ON:**

Both switches are activated simultaneously while in this mode. Shoot-through current, which happens when both switches conduct at the same time and cause a short circuit across the input voltage source, is normally prevented by avoiding this mode.

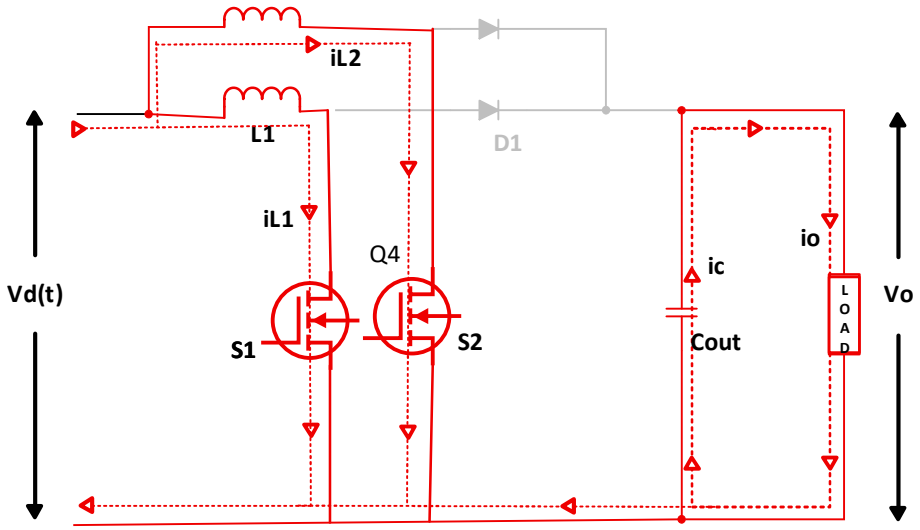

Fig 2.4 Mode 2(S1 & S2 ON).

- **Mode 3 - Switch 1 OFF, Switch 2 ON:**

This mode joins the output capacitor and inductor by activating Switch 2. As the stored energy in the inductor is transmitted to the output capacitor, the output voltage increases. There is still no current on Switch 1.

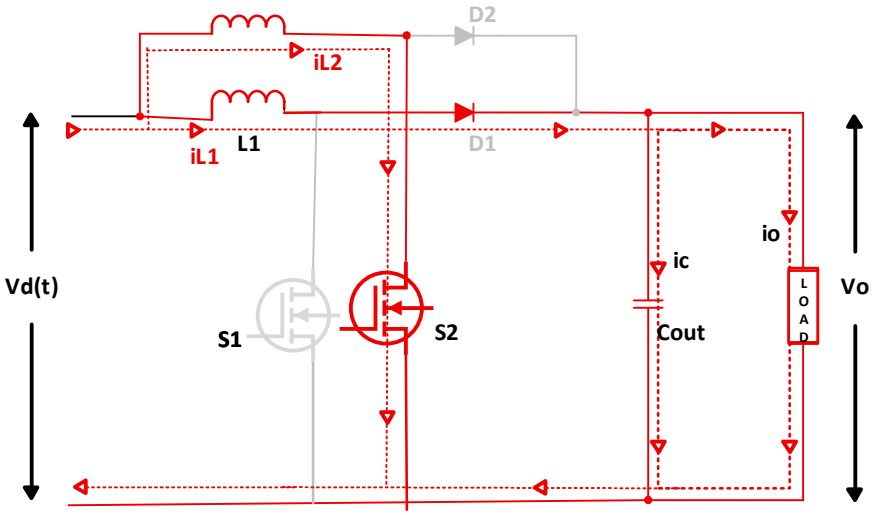

Fig 2.5 Mode 3(D1 & S2 ON).

- **Mode 4: Both switches OFF:**

At this point in the operation of the converter, neither of the two switches is conducting current. The inductor and the output capacitor are both disconnected from the input source. This mode of operation (no switches are conducting current) allows for the elimination of "shoot-through" during the dead time between switching transitions.

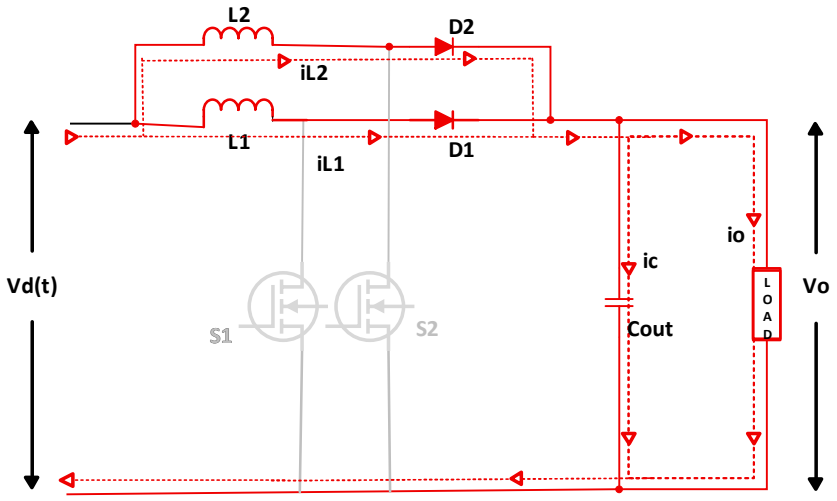

Fig 2.6 Mode 4(S1 & S2 ON).

3.4 SMALL SIGNAL MODELLING

From Fig. 2.3.,

$$\dot{\iota_{l1}} = \frac{V_{in}}{l_1} \tag{2.1}$$

$$\dot{\iota_{l2}} = \frac{V_{in} - V_c}{l_2} \tag{2.2}$$

$$\dot{V_c} = \frac{\dot{i_{l2}}}{c} - \frac{V_c}{Rc} \tag{2.3}$$

$$A_1 = \begin{bmatrix} 0 & 0 & 0 \\ 0 & 0 & -\frac{1}{L_2} \\ 0 & \frac{1}{C} & -\frac{1}{RC} \end{bmatrix}, B_1 = \begin{bmatrix} \frac{1}{L_1} \\ \frac{1}{L_2} \\ 0 \end{bmatrix} \tag{2.4}$$

From fig

$$\dot{\iota_{l1}} = \frac{V_{in}}{l_1} \tag{2.5}$$

$$\dot{\iota_{l2}} = \frac{V_{in}}{l_2} \tag{2.6}$$

$$\dot{V_c} = -\frac{V_c}{Rc} \tag{2.7}$$

$$A_2 = \begin{bmatrix} 0 & 0 & 0 \\ 0 & 0 & 0 \\ 0 & 0 & -\frac{1}{RC} \end{bmatrix} B_2 = \begin{bmatrix} \frac{1}{L_1} \\ \frac{1}{L_2} \\ 0 \end{bmatrix} \tag{2.8}$$

From fig

$$\dot{\iota_{l1}} = \frac{V_{in}}{l_1} - \frac{V_c}{l_1} \tag{2.9}$$

$$\dot{\iota_{l2}} = \frac{V_{in}}{l_2} \tag{2.10}$$

$$\dot{V_c} = \frac{\dot{i_{l1}}}{c} - \frac{V_c}{Rc} \tag{2.11}$$

$$A_3 = \begin{bmatrix} 0 & 0 & -\frac{1}{L_1} \\ 0 & 0 & 0 \\ \frac{1}{C} & 0 & -\frac{1}{RC} \end{bmatrix} B_3 = \begin{bmatrix} \frac{1}{L_1} \\ \frac{1}{L_2} \\ 0 \end{bmatrix} \quad (2.12)$$

State Space Representation:

$$\dot{x} = Ax + Bu \quad (2.13)$$

$$y = qx \quad (2.14)$$

Average State Space Model

The matrix becomes after averaging:

$$A = A_1 * (1 - D) + A_2 * (2D - 1) + A_3 * (1 - D) \quad (2.15)$$

$$A \quad (2.16)$$

$$= \begin{bmatrix} 0 & 0 & \frac{D-1}{L_1} \\ 0 & 0 & \frac{D-1}{L_2} \\ \frac{-(D-1)}{C} & \frac{-(D-1)}{C} & \frac{2*(D-1)}{C*R} - \frac{2*D-1}{C*R} \end{bmatrix}$$

The transfer function matrix is given by

$$G(s) = C((SI - A)^{-1})B \quad (2.17)$$

$$G_{vd}(s) \quad (2.18)$$

$$= \frac{(-L_1L_2Ri_{L1} - L_1L_2Ri_{L2}) * s + L_1Rv_c + L_2Rv_c - DL_1Rv_c - DL_2Rv_c}{CL_1L_2Rs^2 + L_1L_2s + L_1R + L_2R + L_1RD^2 + L_2RD^2 - 2L_1RD - 2L_2RD}$$

2.4 DESIGN OF PARAMETERS

The following parameters were calculated for both boost inductors (L_1 and L_2) and capacitors at the DC Link (C_{dc}). Equation (2.19) is used to calculate boost inductor (L) [2].

$$L = \frac{1}{\%Ripple}\frac{{V_{acmin}}^2}{P_o}\left(1 - \frac{\sqrt{2}V_{acmin}}{V_o}\right)T \tag{2.19}$$

Switching period (T) is obtained as $1/f_{sw}$, duty cycle is denoted by D, minimum AC input voltage by V_{acmin}, and inductor percentage current ripple by ΔI_L.

The output filter capacitor formula is given by (2.20).

$$C_{out} = \frac{DI_{out}}{\Delta V_{out} f_{line}} \tag{2.20}$$

Where Output voltage (V_{out}), output current (I_{out}), and line frequency (f_{line}) are specified in (2.20).

2.5 DUAL LOOP CONTROL

A dual-loop control methodology is used to control the operation of an interleaved boost converter (IBC). This dual-loop control methodology is commonly used in the Power Electronics field to regulate input current and output voltage and is especially useful in applications related to power factor correction (PFC). There are two types of control loops that are utilized as seen in Fig. 2.7. The voltage control loop will respond more slowly than the current control loop, which has a much quicker response time.

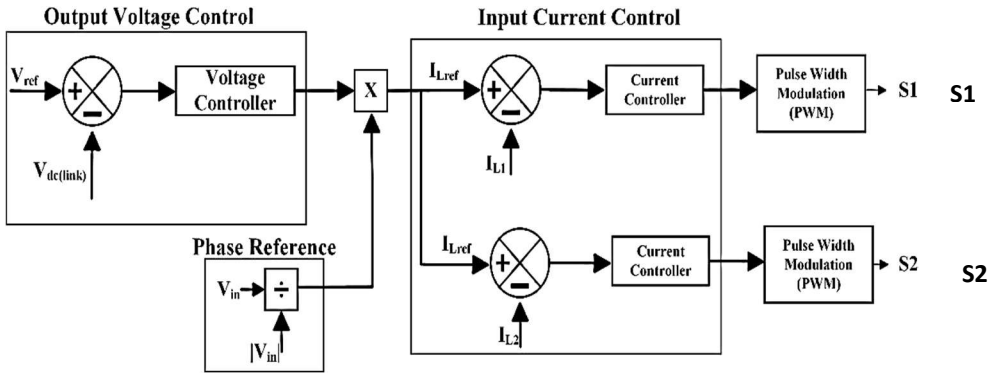

Fig. 2.7 Dual loop control of the Interleaved Boost converter

The inner current control loop has to work fast because it needs to follow the input voltage waveform. Improving tracking speed and accuracy can reduce overall harmonic distortion (THD). The voltage regulation stage maintains the DC link voltage by continually comparing the voltage across the output capacitor with a

reference voltage and sending the resultant error signal to a voltage PI controller. The output of the voltage controller sets the reference level for the inductor current, which is calculated by multiplying the phase reference (usually a sine wave) by the output from the voltage controller. The reference current is compared to the actual current through both of the inductors, and the difference between the actual inductor current and the reference inductor current is used by the current PI controller for each inductor to make gate pulses for the devices required for switching. The output of the current controller is compared to a 50 kHz periodic waveform to produce gate pulses for switching the supporting devices.

2.6 Parameters

Parameter	Values
$V_{in(ac)}$	230 volts
V_o	400 volts
f_s	50KHz
D	>0.5
L	500uH
C	2000 uF
I_o	7.5 amps
P_o	3 KW

Table: 2.1 Parameters of Interleaved Boost PFC

2.7 Simulation Results

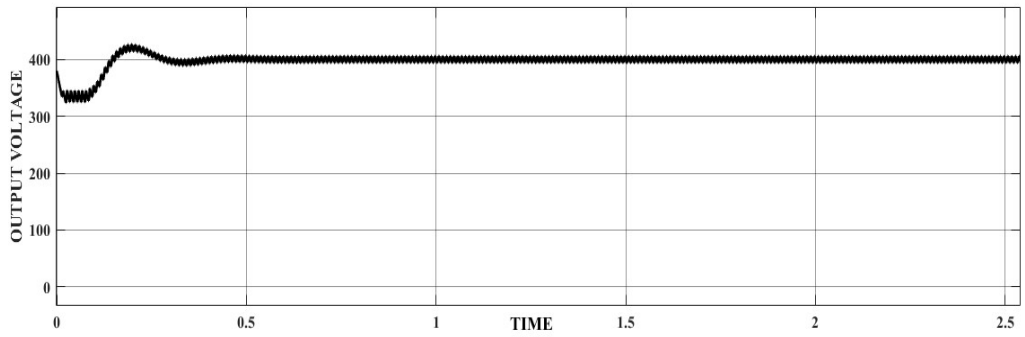

Fig. 2.8 Output Voltage.

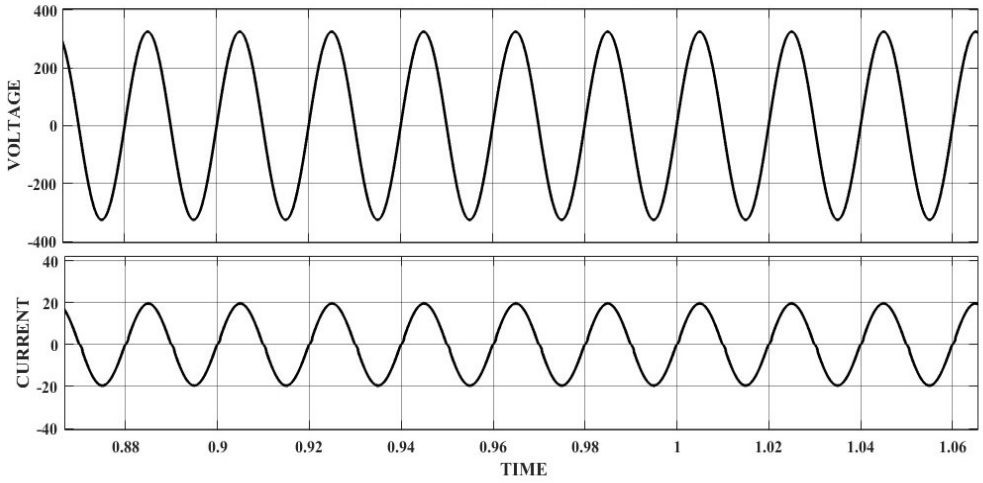

Fig.2.9 Input Voltage and Input Current

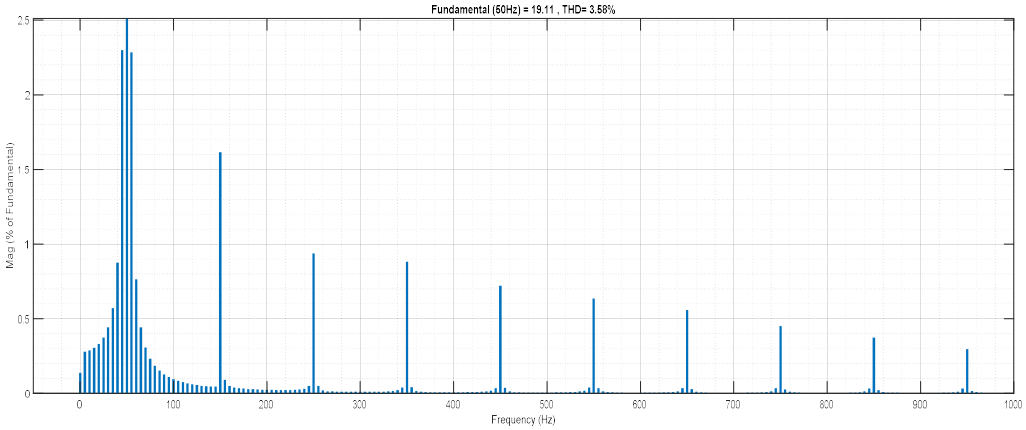

Fig.2.10 Input Current THD (<5%).

Results with Load variation

Load Resistance Varying from 53.33 ohm to 40 ohm therefore Load current varying from 7.50 amps to 10 amps & DC Link voltage is settling to 400 volt with small disturbance hence the closed loop is working perfectly fine

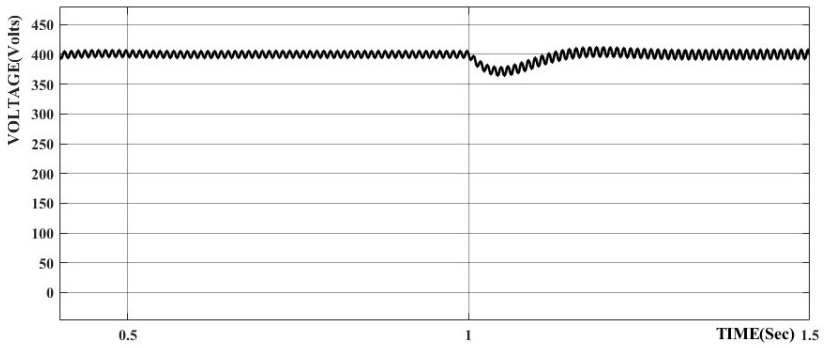

Fig.2.11 Output Voltage with Resistance Decreasing from 53.33 to 40 ohms.

Load Resistance Varying from 53.33 ohm to 40 ohm therefore Load current varying from 7.50 amps to 10 amps & Input Current is increasing with small disturbance remains sinusoidal only hence the Current loop is working perfectly fine.

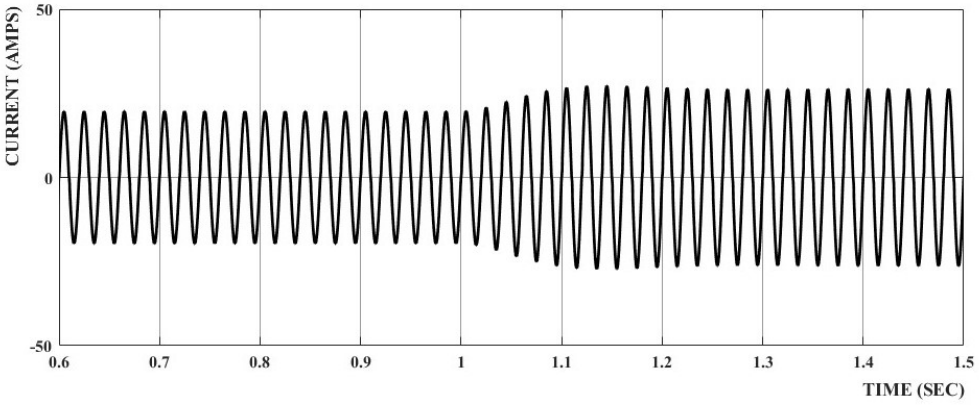

Fig.2.12 Input Current with Load Variation

Results with Line Variation

Line Variation from 230 V ac to 250 V ac.

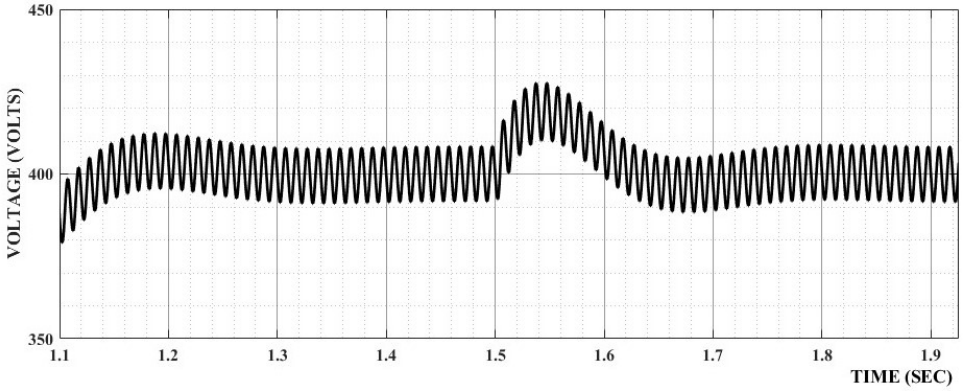

Fig.2.13 Output voltage.

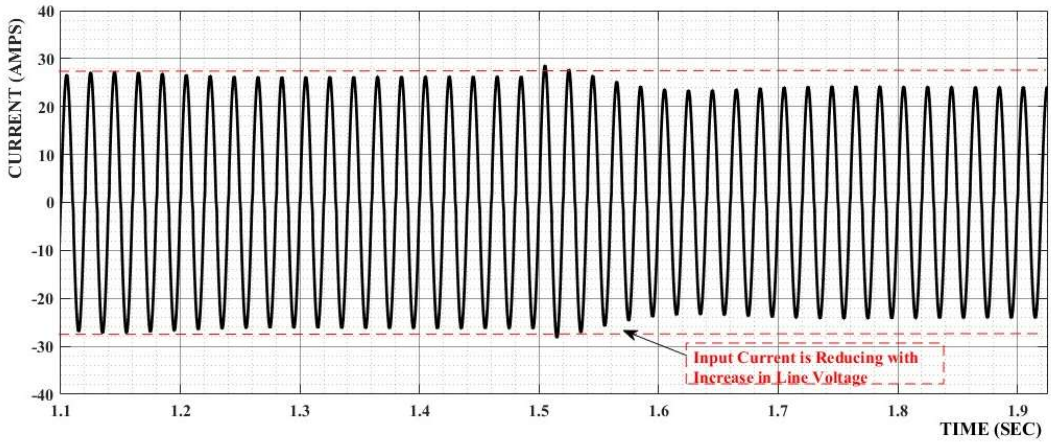

Fig.2.14 Input Current.

Line Current is reducing with Increase in Line Voltage to maintain constant power.

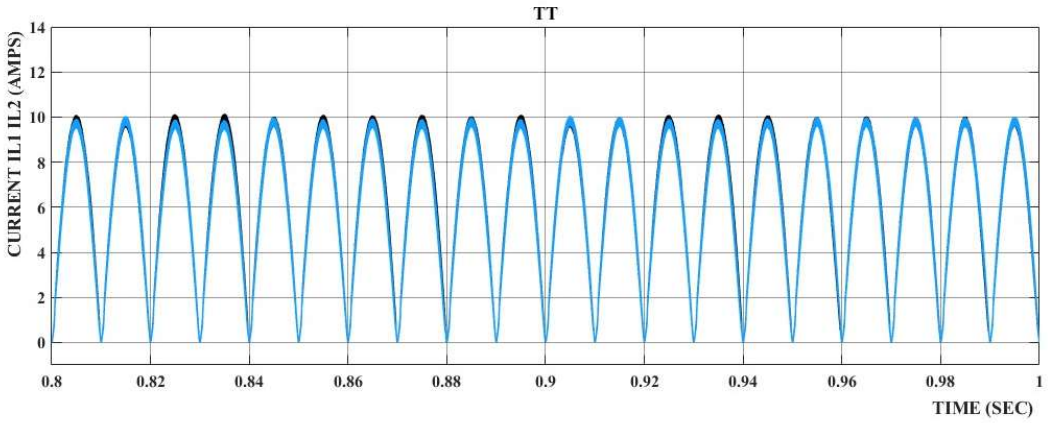

Fig.3.15 Both Inductors Balanced Current.

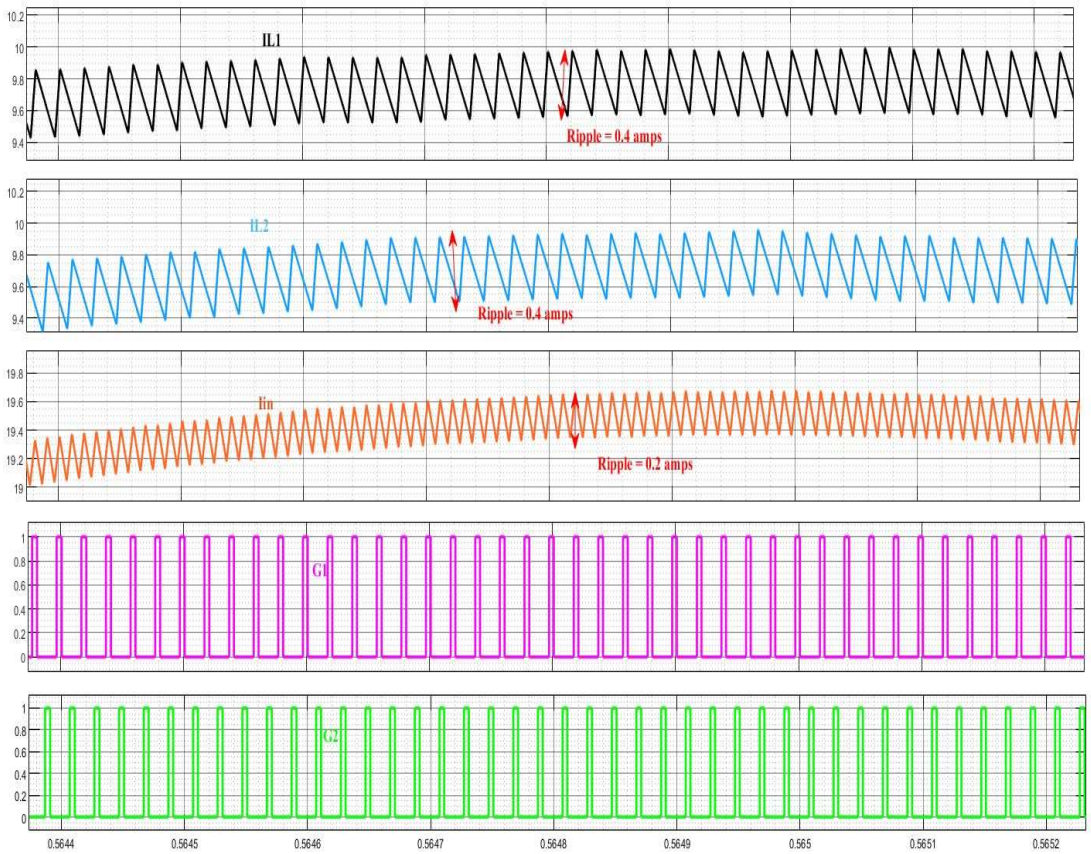

Fig.3.16 Zoomed Version of Both Inductors & Input Current.

2.8 Chapter Summary

This chapter presents an in-depth analysis of the AC-DC power conversion stage, focusing on both the control techniques and component design associated with the interleaved boost converter. A dual-loop control scheme utilizing PID controllers is examined through Small-Signal Modeling to demonstrate how unity power factor and the desired DC link voltage can be achieved. Additionally, the effects of load and grid-side variations are taken into account in the analysis.

CHAPTER 3
DESIGN AND ANALYSIS OF FULL BRIDGE LLC RESONANT CONVERTER

3.1 INTRODUCTION

The rapid advancement of modern power electronics has created an ever-increasing demand for power conversion systems that offer both high efficiency and compactness. Resonant converters are an increasingly attractive option regarding converter topologies; their design takes advantage of soft-switching techniques to greatly reduce switching losses. The LLC resonant converter (named for its two inductors L_m, L_r, and one capacitor - C_r) is seeing a great deal of interest in both academic and industrial research, especially when used in a full-bridge configuration. Traditional hard-switching converters have significant switching losses, particularly at higher switching frequencies due to turn-on and turn-off losses accumulating quickly at higher frequencies. Therefore, the higher switching frequencies result in overall conversion efficiency limits and significant thermal stress on semiconductor devices. The LLC resonant topology overcomes this limitation because; the primary-side switches achieve zero-voltage switching (ZVS) and the secondary-side diodes operate under zero-current switching (ZCS) conditions. As a result of the LLC converter's dual soft switching capability, it is particularly well suited for high frequency operation as it substantially reduces the size of magnetic components and, therefore, the overall size of the overall system [20].

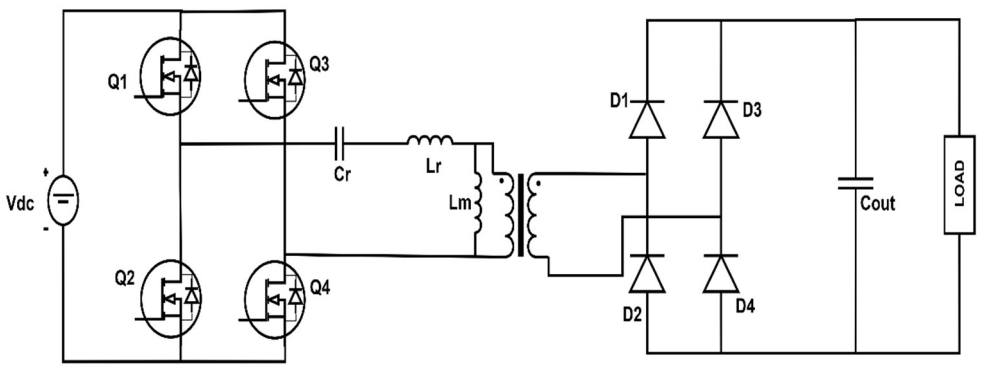

Fig3.1: Full Bridge Resonant LLC Converter

The LLC resonant converter's full-bridge configuration is optimal for use in high and medium-power applications, compared to the half-bridge version. There are a total of 4 active switches used in the full-bridge configuration, which effectively doubles the voltage that can be applied across the resonant tank. To put it another way, the reason that the full-bridge LLC resonant converter is able to handle greater power loadings without increasing component stress proportionally is primarily due to the fact that the full-bridge configuration allows greater Battery-Charging Systems, Server Power Supplies, Electric Vehicle Onboard Chargers, and Renewable Energy Processing Units to have longer-lasting lives than manufacturers would otherwise expect from them.

The fundamental distinction between the LLC type of resonant converter and the various other types of resonant converters is that the LLC converter (also known as the "L, L_M" resonant converter) has two separate resonant frequencies. One frequency is produced by the series resonance of Lr (the resonant inductance) and Cr (the resonant capacitor). The other frequency is produced by the series resonance of both Lr (the resonant inductance) and L_m (the magnetising inductance), in combination with Cr (the resonant Capacitors). This is how the LLC resonant converter can regulate its output by general frequency variation and not by changing the duty cycle. The control technique based on frequency generates significant complications for the analysis, model-building, and closed-loop design of the LLC resonant converter, and requires an in-depth understanding of how to properly configure the LLC converter to perform based on the full frequency supports for the LLC converter during its operation.

To design a full-bridge LLC resonant converter requires careful consideration of resonant tank parameters to set the inductance ratio (L_m/L_r) and the quality factor Q. These parameters have significant effects on voltage gain characteristics, load regulation, and the size of the ZVS operating area. Although the first harmonic approximation (FHA) is relatively simple to use as an analytical method for characterising voltage gain with initial component selection, the method does not provide accurate results far from resonance or under low load conditions. Consequently, time-domain approaches and simulation-based verification will provide complementary methods to determine power switching performance.

The goal of this chapter is to provide a complete analysis and design of a full bridge LLC resonant converter. The chapter will first review the characteristics of the topology and provide an overview of the principles of operation and the waveforms. This principle will be used to derive a model for voltage gain, using frequency harmonic analysis (FHA). The design process will then address the components associated with the LLC converter, including the resonant tank, transformer, and magnetic components. The chapter will also include simulation results to confirm theoretical predictions and evaluate converter performance at various degrees of load and frequency. The chapter will achieve the authors goal of establishing a complete understanding of the LLC resonant converter; therefore, forming a basis for the practical implementation and optimization of a full bridge LLC converter.

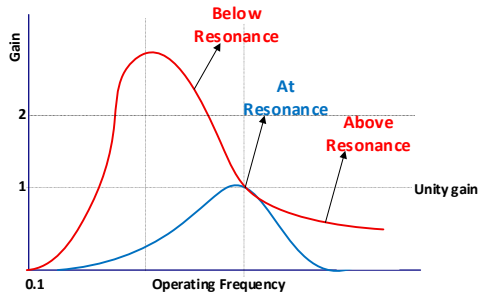

Fig3.2: Different resonant operation modes.

Operation at Resonance

For this operational mode, the switching frequency is set to equal the series resonant frequency ($f_{sw} = f_o$), allowing switches Q1 and Q4 to simultaneously conduct power during the positive half cycle of the applied switching voltage. Because the resonant inductor and capacitor are naturally impedance matched at this frequency, the resulting resonant current has a purely sinusoidal waveform. At t = t1, as switches Q1 and Q4 turn off, the resonant tank current changes and approaches the magnetizing current (I_m). The change in the resonant tank current continues on until after t = t2 (during the period after t1, and before t2, there are no active switches conducting). The fact that the converter operates on a strictly

31

fsw = fo basis means that the converter will not have a very wide output voltage range in which to regulate because the gain will be constant (equal to unity), and frequency deviation from resonance is the primary means of control.

The two purposes of the T1 to T2 intentional Delay Time Period for turning on the Q2 and Q3 devices are:

(1) to allow for the complete discharge of the junction capacitance of the incoming switches through the circulating magnetizing current to create Zero Voltage Switching (ZVS) conditions at the time of the turn-on from T1 to T2, and

(2) to allow for the natural decay of the diode current to 0 within the same time period, allowing for Zero Current Switching (ZCS) of the rectifier diodes to avoid Reverse Recovery Loss.

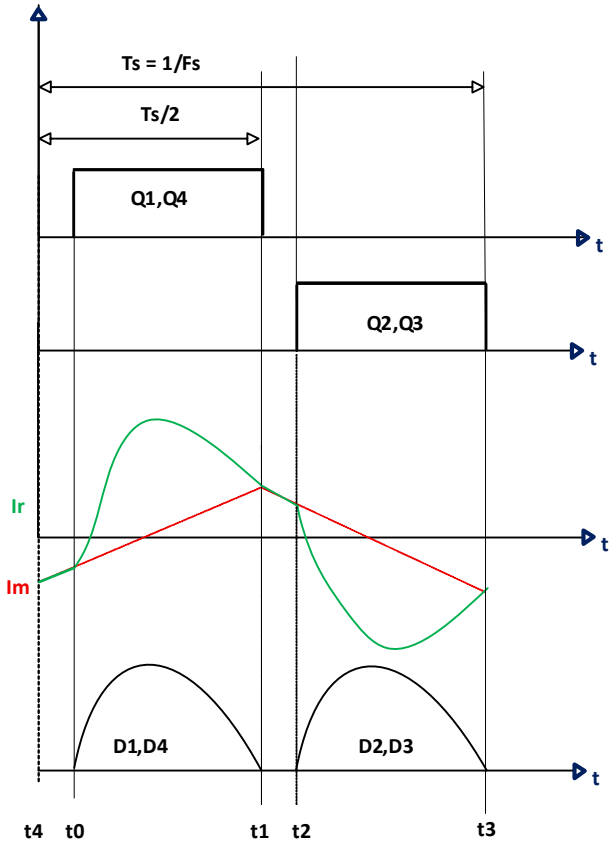

Fig3.3: Operation at Resonance

Operation below Resonance

The condition depicted in Fig 3.2 shows that when the switching frequency (f_{sw}) is less than the resonant frequency of the system, the amount of circulating current increases and switching device losses also increase due to the continuous

nature of the diode current. Therefore, if the converter is to maintain its ZVS ability, it should operate at its maximum switching frequency less than the resonant frequency.

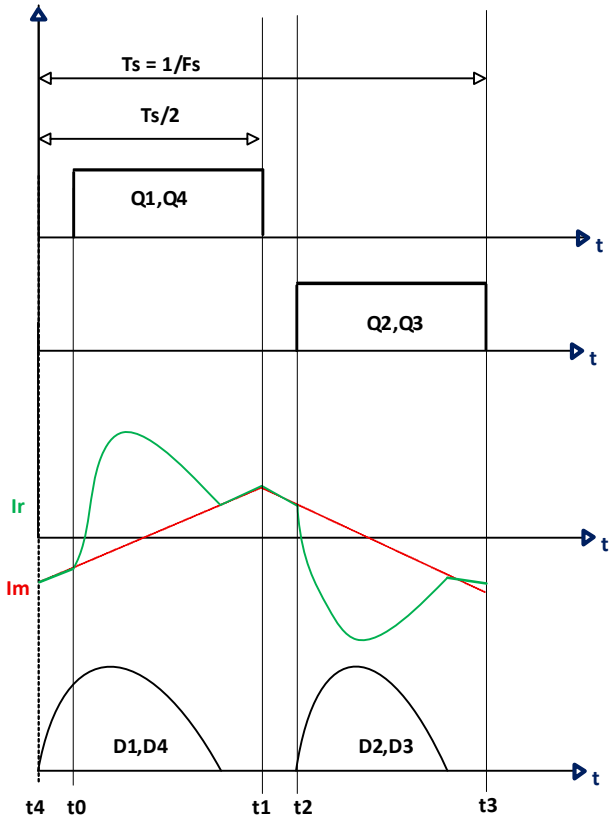

Fig3.4: Operation Below Resonance

Operation above Resonance

Conversely, when the switching frequency (f_{sw}) is set greater than the resonant frequency (f_o), the switching period will be shorter than the natural resonance period. This means that there won't be enough time for the resonant current to complete a full half cycle before the next switch occurs. As a result, the resonant current will remain continuous over the switching period and will very closely follow a sinusoidal shape with no zero crossings between transitions. There are some major advantages in having such an uninterrupted current profile from the point of view of energy circulation in the resonant circuit. Because the wave does not stay at zero for long unlike what happens in the clamping effect that occurs below resonance, the peak as well as the rms values of the resonant current are relatively low. As a result, the power losses through the conducting path of the

switches become relatively low due to lower rms current values through the MOSFET switches.

None the less, there is a notable limitation that arises as a result of this operational region from the secondary side of the converter. Since switching occurs prior to the natural decay of the resonant current to zero, there is forced commutation of the diode current on the secondary side, hence failing to turn off at zero current. The current in the diode gets suddenly cut off when it is still flowing through the diode, hence making hard commutation possible, resulting in the creation of significant reverse-recovery losses in ordinary p-n junction diodes. Therefore, the requirement of using Schottky diodes or synchronous rectifiers on the secondary side of the circuit due to the negligible reverse recovery properties cannot be overlooked for above resonance operations.

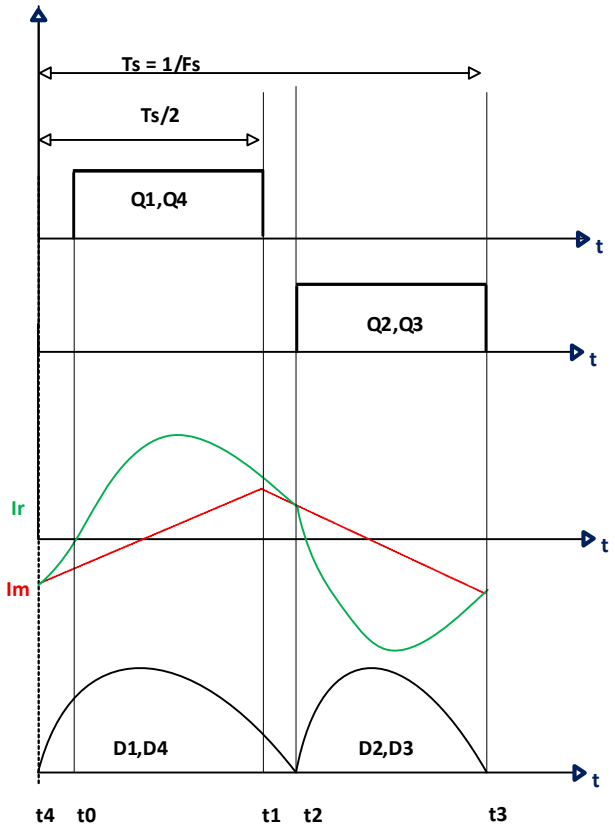

Fig3.5: Operation Above Resonance

3.2 Modes of Operation

It can be said that the operating cycle of the LLC resonant full bridge converter may be divided into four modes, including the positive cycle mode, the negative cycle mode, and two others called the free-wheeling mode. It should be noted that the classification of the above modes is made according to the period of a single switching cycle.

Positive Cycle Operation Fig. 3.6

During the positive cycle, both gates are turned-on at the same time for the diagonal switches Q1 and Q4. The proper conduction of the two switches generates the positive square-wave pulse at the input of the resonant tank circuit. The generated pulse results in the generation of resonant current in the positive direction through the series combination of Lr, Cr and Lm, where the active energy transfer takes place from the input side through the transformer to the output side of the converter.

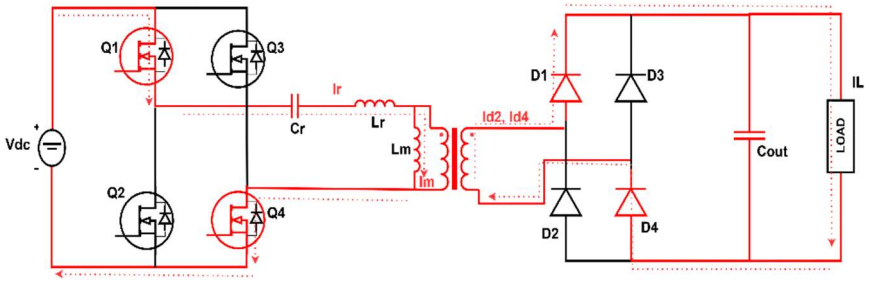

Fig3.6: Positive Cycle

Negative Cycle Operation Fig. 3.7

Under the negative cycle, the gate pulses are reversed to flow to the other diagonally opposed switches Q2 and Q3, while Q1 and Q4 switches are off. The on-state conditions of Q2 and Q3 create a negative half-cycle square wave at the input to the resonant tank, which flows in the reverse direction into the resonant current. Energy transfer occurs between the primary and secondary sides of the circuit, but just as in the positive cycle, only in a reversed polarity of the transformer volt-second application. Both the positive and negative cycle phases make up the stages where active power transfer takes place within the converter.

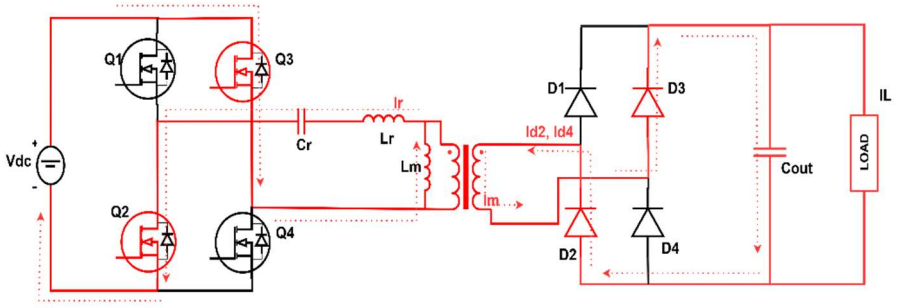

Fig3.7: Negative Cycle

Freewheeling Mode Fig. 3.8

During the operation of the resonant period, there will come a time when the amplitude of the resonant current through the tank starts reducing and tends to be equal to the amplitude of the magnetizing current Im. In this case, the sum total of the current that can be transferred to the second winding is reduced to zero because the magnetizing current flows in the first winding only. The sub-period does not transfer any energy to the second winding; hence, the load on the output is solely dependent on the energy from the output filter capacitor.

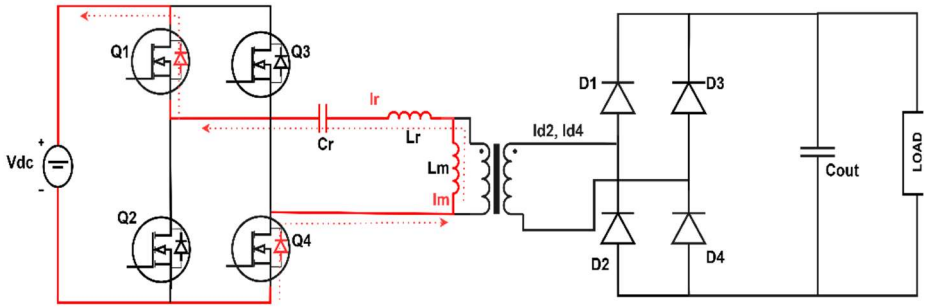

Fig3.8: Freewheeling Cycle

Freewheeling Mode for Positive Magnetizing Current Fig. 3.9

After undergoing the switching process outlined above, the power supply unit is brought into the freewheeling state with regard to the positive polarity of the magnetic current. At this point, the magnetic inductance of the current freewheels through the body diodes of the switch pair that is going to be turned on, resulting in the zero voltage level on these components. The dead time freewheeling is the way in which the zero voltage switch on of the primary side switches is accomplished.

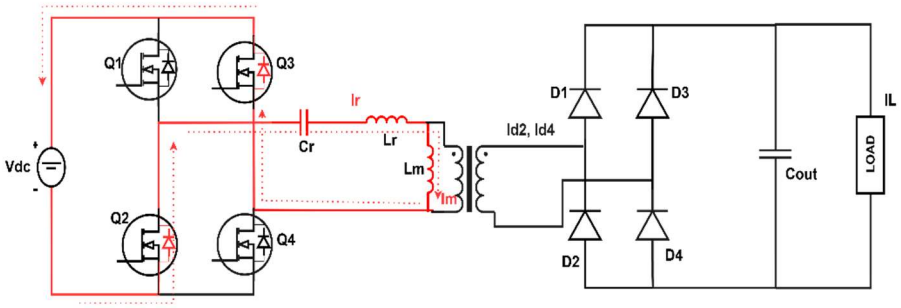

Fig3.9: Freewheeling Cycle

3.3 DESIGN OF FULL BRIDGE LLC RESONANT CONVERTER

The LLC resonant converter is suitable for analysis using a closed-form analytic approach owing to its suitability for FHA analysis. The concept of FHA is based on the idea that, as a consequence of the characteristics of the filter created by the resonant tank circuit, it reacts mainly to the first harmonic of the applied square wave excitation and filters out all other higher harmonics in such a manner that their effect becomes negligible. Therefore, the square wave voltage applied to the resonant tank at the output of the full bridge inverter can be assumed to consist of only its fundamental sine wave.

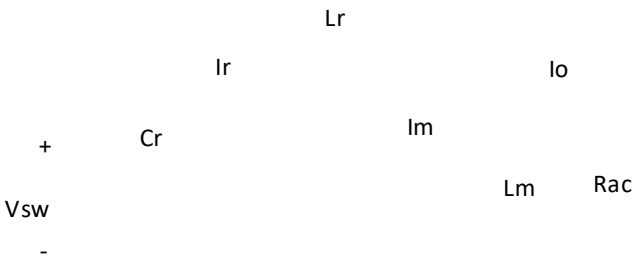

Fig3.10: Series Resonant LLC Equivalent Circuit

The gain is calculated as:

$$Z_p = \frac{1}{j\omega C_r} + j\omega L_r \tag{3.1}$$

$$Z_s = \frac{1}{\frac{1}{j\omega L_m} + \frac{1}{R_o'}} \tag{3.2}$$

$$Z_s = \frac{1}{\frac{1}{j\omega L_m} + \frac{1}{R_o'}} \tag{3.3}$$

$$\frac{V_o'}{V_{in}'} = \frac{Z_p}{Z_p + Z_s} = \frac{1}{1 + \frac{Z_s}{Z_p}} \tag{3.4}$$

$$= \frac{1}{1 + \left(\frac{1}{j\omega C_r} + j\omega L_r\right)\left(\frac{1}{j\omega L_m} + \frac{1}{R_o'}\right)} \tag{3.5}$$

$$= \frac{1}{1 + \frac{L_r}{L_m} - \frac{1}{\omega^2 L_m C_r} + j\left(\frac{\omega L_r}{R_o'} - \frac{1}{\omega C_r R_o'}\right)} \tag{3.6}$$

$$\omega = 2\Pi f, \omega_o = \frac{1}{\sqrt{L_r C_r}}, Q = \frac{1}{R_o'}\sqrt{\frac{L_r}{C_r}} \tag{3.7}$$

$$\frac{V_o'}{V_{in}'} = \frac{1}{1 + \frac{L_r}{L_m}\left(1 - \frac{{\omega_o}^2}{\omega^2}\right) + jQ\left(\frac{\omega}{\omega_o} - \frac{\omega_o}{\omega}\right)} \tag{3.8}$$

$$\frac{|V_o'|}{|V_{in}'|} = \frac{1}{\sqrt{\left(1 + \frac{L_r}{L_m}\left(1 - \frac{{\omega_o}^2}{\omega^2}\right)\right)^2 + Q^2\left(\frac{\omega}{\omega_o} - \frac{\omega_o}{\omega}\right)^2}} \tag{3.9}$$

Design Steps:

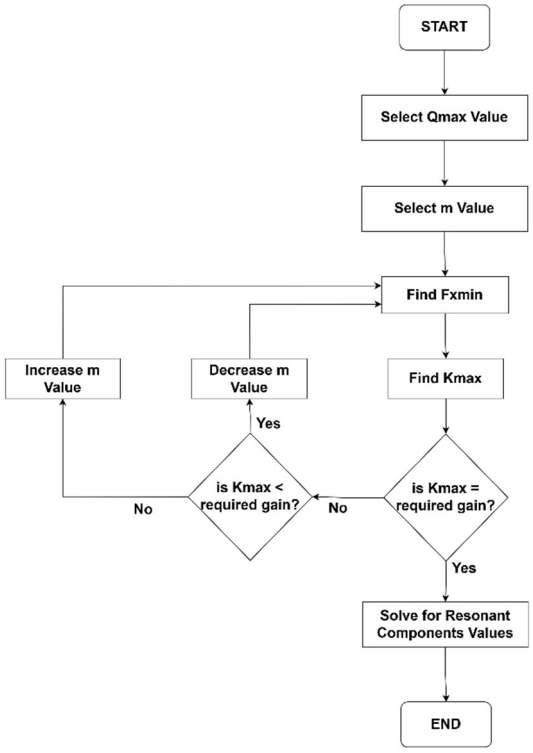

Fig3.11: - Designing steps of LLC Resonant Circuit

Step 1: Selection of the Maximum Quality Factor Q_{max}

The quality factor Q is a load-dependent parameter defined as:

$$Q = \frac{1}{R_{ac}}\sqrt{\frac{L_r}{C_r}} \tag{3.10}$$

The gain is maximum at the maximum load and reduces with the reduction in load. Gain at Q = 0.3 provides better performance in terms of obtaining high boosting gain but necessitates a broad operating frequency range for obtaining minimum gain, which in turn leads to more switching losses. A relatively high value for gain at Q = 1.0 needs a small frequency change in order to meet the minimum gain condition but cannot meet the target gain. A moderate Q value, for example, at Q = 0.5 is ideal because both minimum and maximum gains can be obtained within an appropriate frequency variation range.

The point to note here is that Q_{max} should not be used as the design variable for reaching maximum gain in the first instance. Rather, a moderate Q_{max} should be chosen, and the maximum gain should be met using the inductance ratio parameter m as described in the next step.

Step 2: Selection of the Inductance Ratio m

The inductance ratio m is a static design parameter defined as:

$$m = \frac{L_r + L_m}{L_r} \tag{3.11}$$

Smaller values of m result in greater peak gain and narrow modulation range. This can be useful in cases where wide input voltages are needed. But smaller value of m indicates lower magnetizing inductance L_m, hence resulting in an increase in ripple in magnetizing current, increasing the loss in circulating energy and switching conduction in primary side switches.

An appropriate value of m is first chosen in the range 6 – 10 and later optimized to the maximum possible value of m that fulfils the maximum gain criteria under worst operating conditions.

Step 3: Determining the Minimum Normalized Switching Frequency

After deciding upon Q_{max} and choosing a value of m, the subsequent requirement is to find out the minimum normalized switching frequency f_{nmin} that ensures inductive operation of the resonant tank regardless of the load variation. As inductive operation is the requirement for obtaining ZVS condition of the primary side switches, this limit needs to be defined prior to fixing other design parameters of the resonant tank.

This value will equal the point corresponding to maximum gain on the graph of Q_{max}. As it would be undesirable for the converter to operate beyond this frequency value, the minimum normalized switching frequency can be computed from the differentiation of the voltage gain equation relative to fn

Step 4: Verification of Maximum Voltage Gain

After determining the minimum normalized switching frequency, the next step would be the determination of the maximum possible gain K_{max}, which would

serve as the basis for ensuring that the assumed value of m is adequate to satisfy the gain requirements at full load. This can be done by solving for K using the minimum frequency and given Q_{max} and m values:

$$K_{max} = M(f_{n,min}, Q_{max}, m)$$

This is either calculated analytically using the expression for FHA gain or found graphically as the highest point on the Q_{max} curve.

The result obtained from this verification process decides whether the next phase of the design will proceed in the correct way, as stated in the design flow chart above. The decision made is based on the comparison between the obtained K_{max} and the desired maximum gain. If the obtained K_{max} is below the required maximum gain, the value of m needs to be lowered and Steps 3 and 4 repeated since lower values of m yield higher gain as calculated in Step 2. Alternatively, if the obtained K_{max} exceeds the desired maximum gain significantly, m needs to be increased and the process repeated again. The increased value of m results in the reduction of magnetizing current ripple and circulating energy, and hence higher efficiency of the converter without breaking the gain limit.

Step 5: Calculation of Resonant Tank Component Values

With the optimization for m and Q_{max} accomplished, the tank components' values can now be found explicitly. First, the equivalent AC resistance seen at the primary side is calculated from output power, output voltage, and transformer turn ratio as follows:

$$R_{ac} = \frac{8}{\Pi^2} \frac{{N_p}^2}{{N_s}^2} \frac{{V_o}^2}{P_{omax}} \tag{3.12}$$

Resonant inductance Lr and resonant capacitance Cr are next found by solving jointly for the definitions of the quality factor and series resonant frequency:

$$Q_{max} = \frac{\sqrt{L_r/C_r}}{R_{ac,min}} \tag{3.13}$$

$$f_r = \frac{1}{2\Pi\sqrt{LC}} \tag{3.14}$$

$$m = \frac{L_r + L_m}{L_r} \tag{3.15}$$

L_m is finally calculated from optimized Lr through m.

It should be observed that the series resonant frequency fr does not have any role of a parameter constrained in the design procedure above because its value will have nothing to do with the maximum voltage gain or the regime of operation. The only thing that matters about fr is its influence on power density, core losses of magnetics, and losses during switching. A high value of fr decreases the dimensions of magnetics, including the transformer, but increases demands on controlling the switching losses.

3.4 Control of Full Bridge Resonant LLC Converter

The following section describes the designing and implementation of closed-loop voltage controller used in the full bridge LLC resonant converter having power rating of 3 kW and output voltage of 48V. The voltage regulation is achieved through the use of variable frequency modulation approach, where the frequency with which the four primary side switches Q1, Q2, Q3 and Q4 turn on or off changes to ensure output voltage regulation. It should be noted that throughout this discussion, the source of input voltage is DC voltage of 400V as opposed to the Interleaved boost PFC stage.

Voltage Control of LLC resonant converter

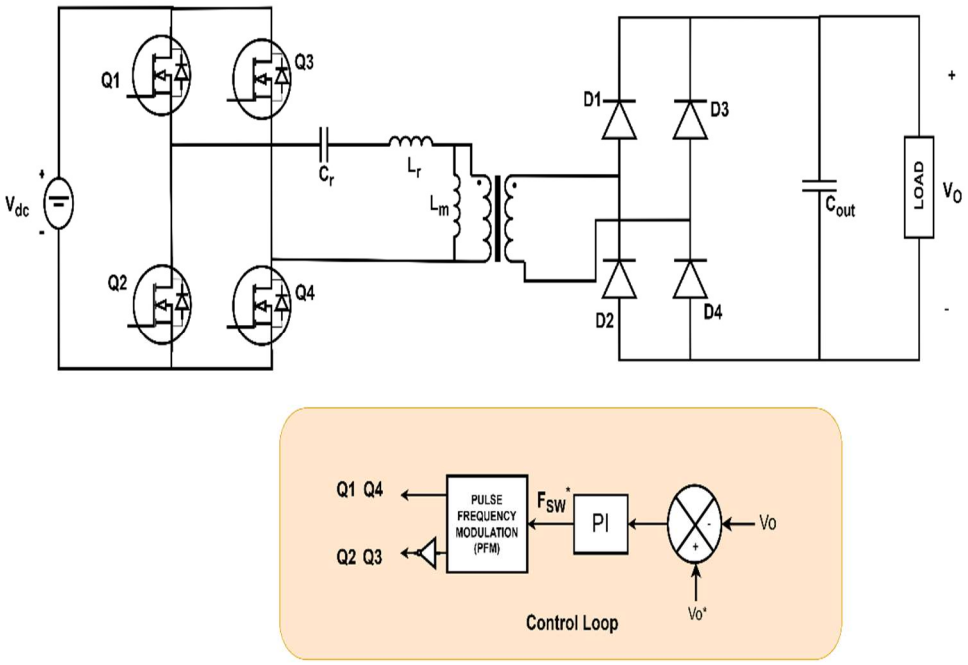

Fig3.12: Voltage Control of LLC Resonant Converter

The closed-loop voltage regulation of the full-bridge LLC resonant converter is achieved through a proportional-integral (PI) voltage control loop, which generates a variable switching frequency command $f_{sw}{}^{*}$ as its output. The control law governing this frequency command is expressed as:

$$f_{sw}{}^{*} = \{K_{pv}\,(V_o{}^{*} - V_o) + K_{iv} \int (V_o{}^{*} - V_o)dt\} \tag{3.16}$$

Where K_p, K_i are PI Controller Gains for voltage loop.

In pulse width modulation, a constant switching frequency is used, and the duty ratio varies continually for controlling the output voltage. Although the technique reduces the complexity of the control system, it suffers from a weakness when operating at light load levels; the constant switching frequency causes the ratio between switching losses and output power to be very high.

This problem is solved through pulse frequency modulation by using the opposite approach; that is, a fixed duty ratio of 50% is employed along with a varying switching frequency according to the load requirements. There are two ways of implementing the modulation; either the on-time of the pulse remains constant while the off-time is variable, or vice versa. If the load level is high, then the switching frequency will be increased for providing the desired power to the load. On the other hand, the frequency can be decreased when the load level is low; fewer transitions reduce switching losses. Pulse frequency modulation is especially effective for regulating the output voltage of LLC resonant converters.

In PWM the output voltage is function of duty ratio (D)

$$V_o = f^{n}(D) \tag{3.17}$$

In PFM the output voltage is function of switching frequency (f_{sw})

$$V_o = f^{n}(f_{sw}) \tag{3.18}$$

3.5 Parameters

Parameter	Values
V_{dc}	400 volts
V_o	48 volts
P_o	3 KW
F_s	100KHz
D	>0.5
L_r	18 uH
C_r	135 nF
L_m	90 uH
C_o	220 uF

Table3.1: Parameters for Full Bridge Resonant LLC

3.6 Result

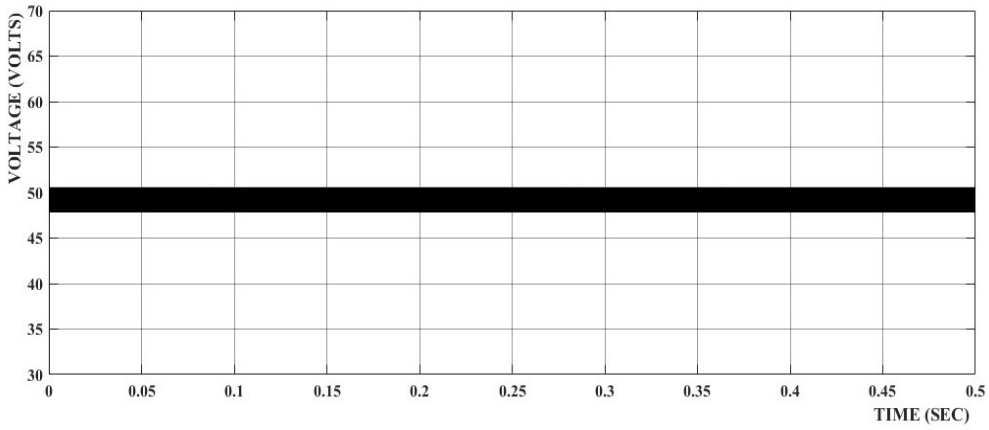

Fig3.13: Output Voltage

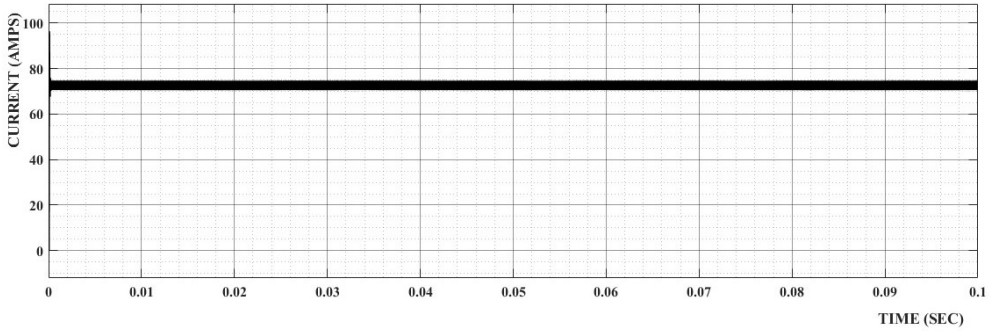

Fig3.14: Output Current

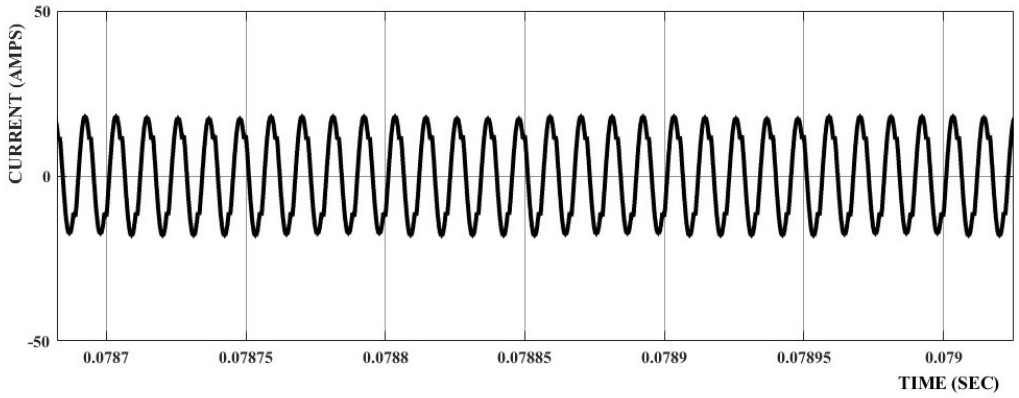

Fig3.15: Resonant Current (amps)

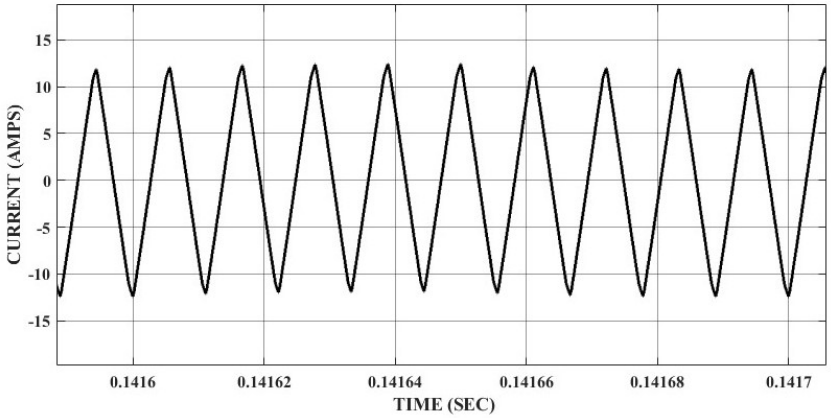

Fig3.16: Magnetizing Current (amps)

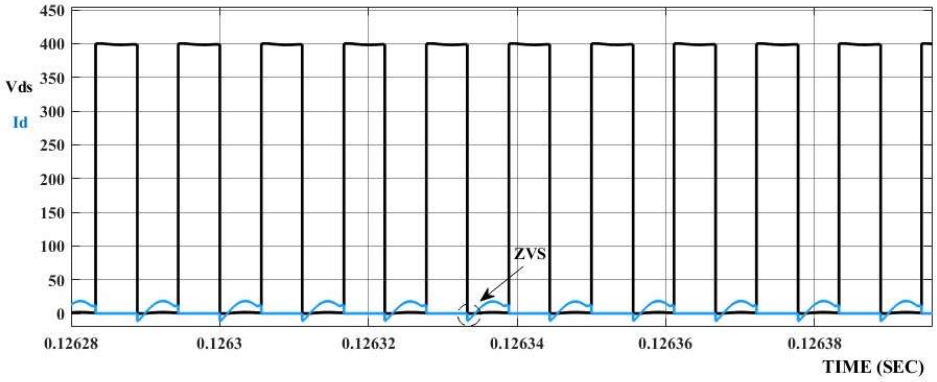

Fig3.17 : Drain to Source voltage & Drain Current

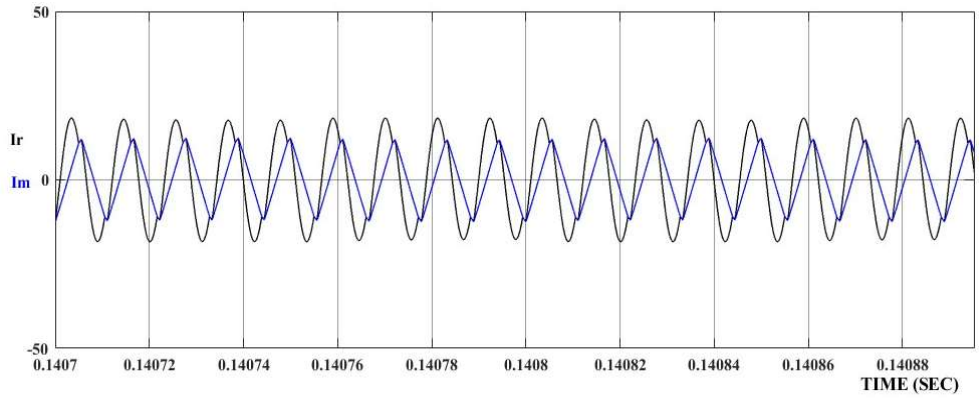

Fig3.18 : Resonant Tank Current Characteristics.

3.7 Chapter Summary

The analysis of the full-bridge LLC resonant converter covered extensively in this chapter included an in-depth study of the behaviour of the circuit in three different frequency domains, i.e., at resonance, sub-resonance, and super-resonance, focusing mainly on the switching performance, resonant current waveforms, and soft switching conditions applicable in each case.

In this regard, the four unique modes of operation of the full-bridge structure were studied in depth to provide an insight into how power is coupled from the primary winding to the secondary winding using active conducting periods while the freewheeling periods ensure zero voltage switching at the primary-controlled switch.

After that, the detailed design procedure of the resonant tank included the determination of Q_{max}, the optimum inductance ratio, the minimum normalized frequency, validation of maximum voltage gain, and finally determining the value of Lr, Cr, and L_m. Throughout this design process, a lot of attention was devoted to ensuring the conversion runs at inductive region irrespective of input voltage and load, hence ensuring ZVS at primary switches.

CHAPTER 4
TWO STAGE INTERLEAVED BOOST PFC FED FULL BRIDGE LLC RESONANT CONVERTER

4.1 INTRODUCTION

As the need for miniaturized AC-DC power conversion has increased significantly, the cascade combination of multiple converters has become an active area of research by virtue of its benefits as compared to single stage conversions. In this research, an interleave boost PFC converter and full bridge resonant LLC converter have been integrated as a two-stage power conversion system with a rating of 3 kW. In the first stage, an AC supply of 230 V has been converted to a regulated DC voltage level of 400 V through the use of an interleaved boost PFC converter that operates with a double loop control scheme to provide near unity power factor in addition to regulating the DC bus voltage. A full bridge resonant LLC converter has been used in the second stage for stepping down the 400 V DC bus voltage to a regulated 48 V output through the use of PFM voltage control scheme.

While each stage has been designed and analysed in detail through previous chapters, their sequential operations create dependencies which need to be investigated in depth. In this regard, the 400 V DC link acts as the connecting medium for the two stages, and any transient deviation caused by the PFC dual loop control will affect the frequency and voltage amplification of the LLC topology. The current chapter analyses the combined performance of the entire two-stage converter, covering aspects such as power transfer, voltage stress, and efficiency. This provides a basis for the implementation and testing discussed in the subsequent sections.

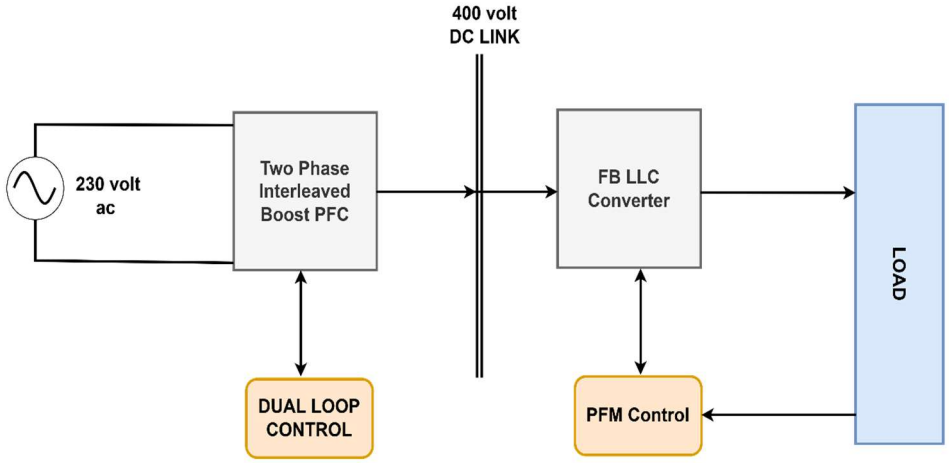

Fig4.1: Block Diagram of Cascaded Network.

4.2 CIRCUIT DESCRIPTION OF CASCADED NETWORK

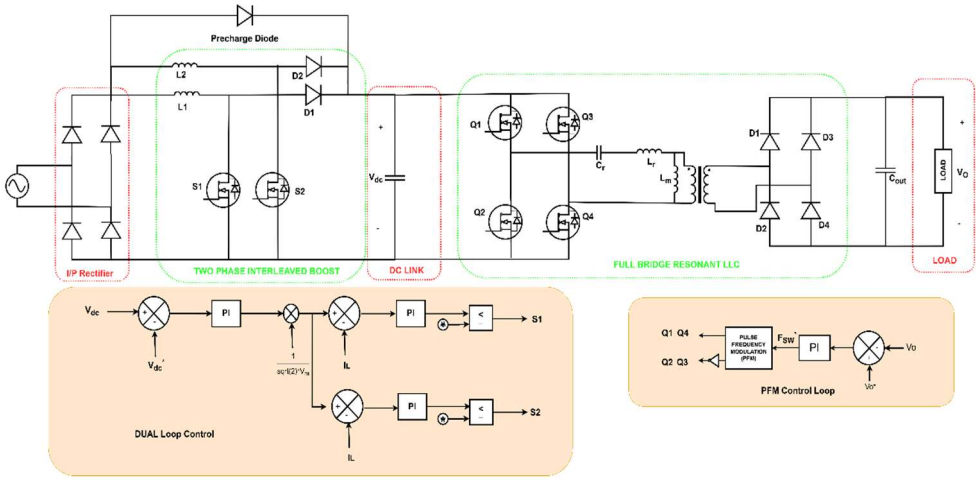

Fig4.2: Circuit & Control Diagram for Cascaded Converter.

The 3 kW two stage AC-DC converter design involves the use of an interleaved boost power factor correction converter connected in cascade with a full bridge resonant LLC converter. The 400V DC bus acts as the point of connection between these two converters such that the power factor correction converter serves as the input side while the LLC converter serves as the output side. Both converters process an input power source of 230V AC mains and deliver a regulated 48V DC output.

For the operation of the first stage which is made up of two parallel operated boost converter cells, the control scheme adopted is a dual loop control scheme. For this case, the first loop, which is the voltage control loop measures the 400V DC bus and develops a reference signal based on the difference between the measured value of voltage and desired reference. Then this reference signal feeds into the current control loop which controls the shape of inductor current in each cell in a way that the resulting current waveform has a sinusoidal envelope which matches that of the rectified input voltage wave form, thereby making it operate at near unity power factor.

Stage two uses an LLC resonant full bridge converter to convert the 400V DC bus voltage to a high-frequency AC voltage, which is fed into the LLC resonant tank comprising the series resonant inductance, resonant capacitor, and transformer magnetizing inductance. This configuration allows for ZVS operation for the primary switches and ZCS operation for the secondary diodes. This increases conversion efficiency in the system. The 48V DC output is controlled using a PFM voltage control scheme whereby the switching frequency of the resonant circuit varies relative to the resonant frequency according to the error of the output voltage. If the error indicates the tendency of the output voltage to decrease, the voltage gain is increased, while a tendency towards rising voltage lowers the voltage gain. The 400V DC bus serves as a decoupling link between the two control loops, hence providing independent operation of dual-loop PFC control and PFM voltage control.

4.3 Parameters

Parameter	Values
$V_{in(ac)}$	230 volts
V_{dc}	400 volts
F_s	100KHz
D	>0.5
L_r	6 uH
C_r	400 nF
L_m	30 uH

L_1	560 uH
L_2	560 uH
C_o	220 uF
V_o	48 volt
P_o	3 KW

Table4.1: Parameters for Cascaded Network

4.4 Results

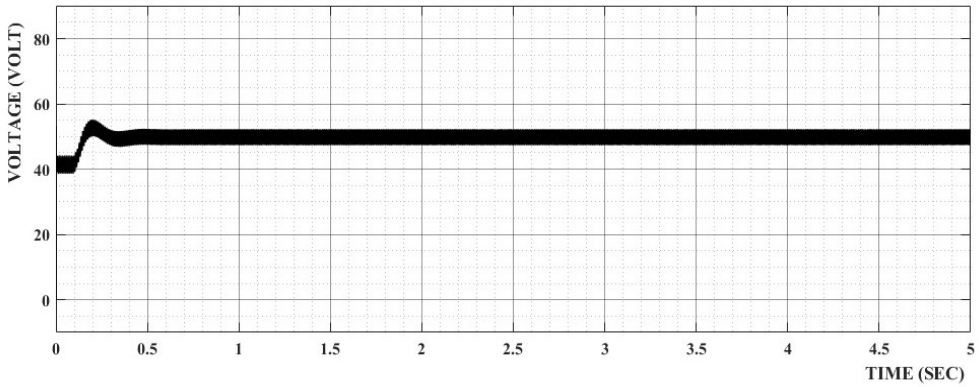

Fig 4.3: Output Voltage (volt)

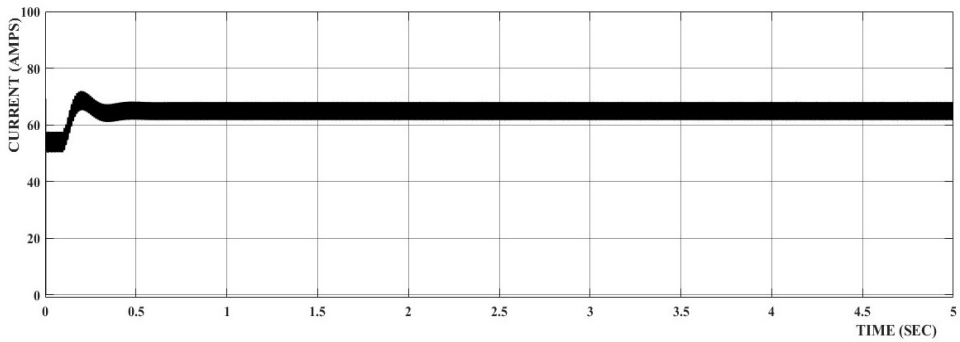

Fig4.4 : Output Current

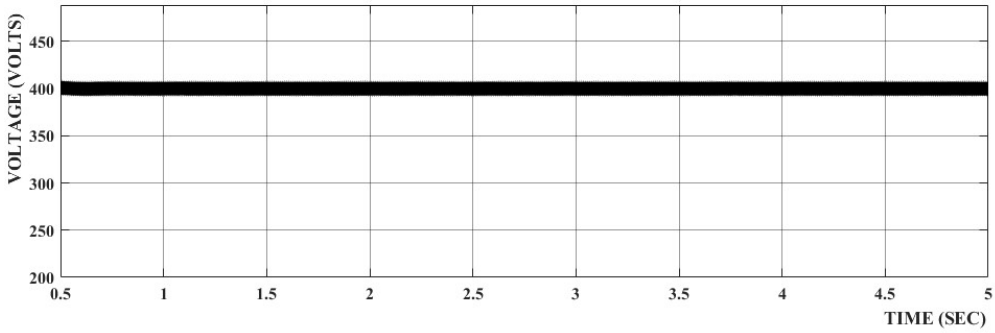

Fig4.5: DC Link Voltage (volt)

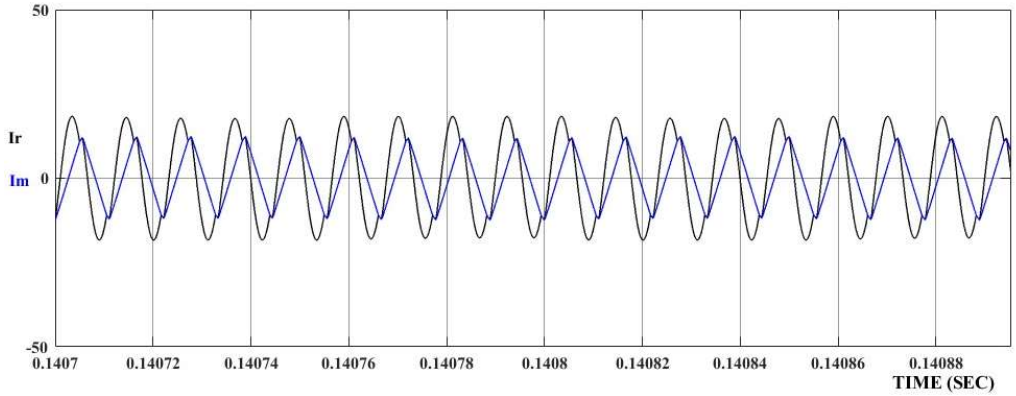

Fig4.6: Resonance Charaterstics

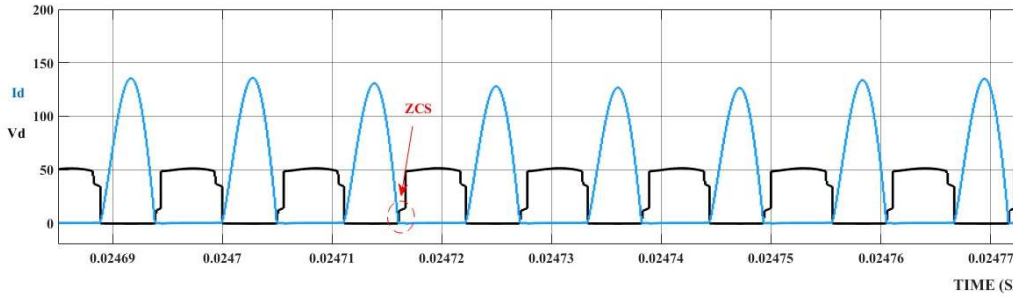

Fig4.7 : Secondary Side Rectifier Diode's Turn ON

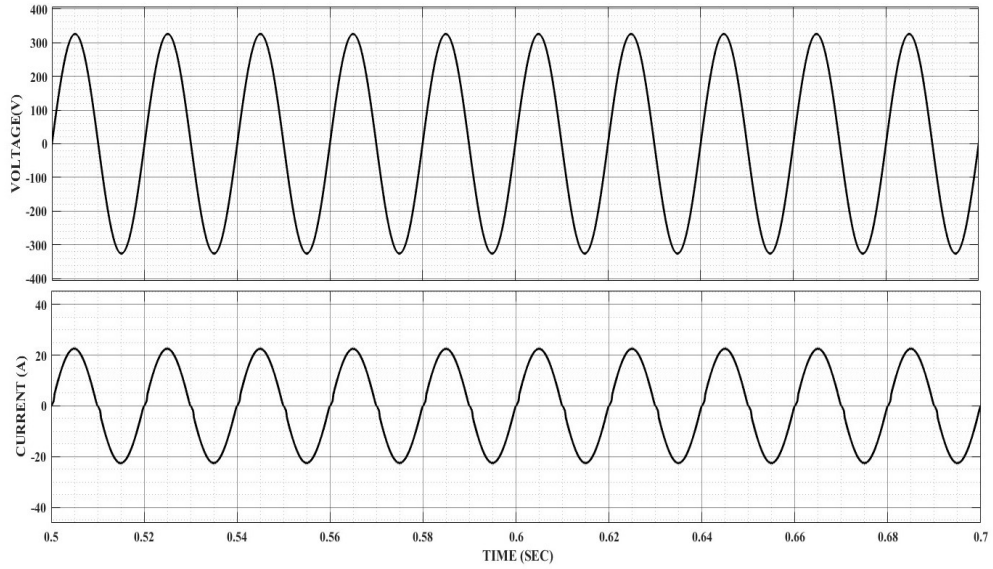

Fig 4.8: Input Voltage and Input Current

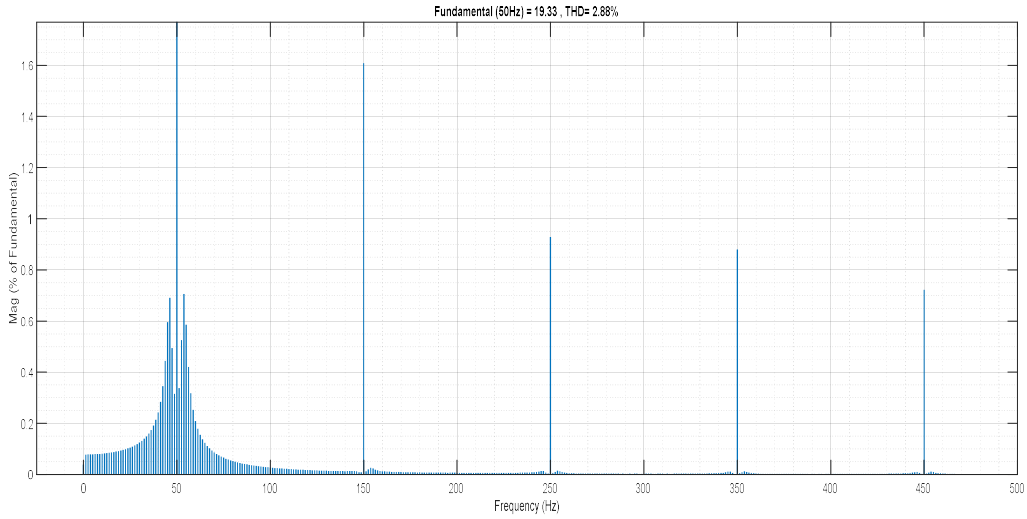

Fig4.9: Input Current THD

4.5 Conclusions

In this chapter, the operation of the two stages AC-DC cascaded conversion system has been elaborated on by describing the operation of both the interleaved boost PFC and the full-bridge resonant LLC converters together to form one

complete 3 kW power supply circuit for generating a regulated 48 V DC output from a 230 V AC input using an intermediary 400 V DC bus voltage level.

The simulation results of the integrated system have verified that all the operations are successful according to their requirements. In the case of the interleaved boost PFC stage, the DC bus voltage is regulated to 400 V. Meanwhile, its input current follows a sinusoidal wave reference signal, resulting in a THD less than 5%. At the same time, the full-bridge resonant LLC converter successfully regulates the 48 V DC output voltage according to the requirement despite changes in the input DC bus voltage and loading conditions due to its PFM control technique.

These findings indicate that the proposed cascaded structure, with control schemes being independent yet complementary to each other, can successfully achieve power quality in the input stage, intermediate bus voltage stabilization, and tight regulation of DC output voltages all together. In particular, having an intermediate 400 V DC bus helps effectively isolate the dynamics of both circuits, hence avoiding any meaningful interference between the PFC dual loop control and LLC PFM voltage control loops. On balance, the proposed solution represents quite a balanced combination of efficiency, power density, and ease of control, laying the foundation for implementation and testing that will follow in the next chapter.

CHAPTER 5
HARDWARE IMPLEMANTATION

5.1 INTRODUCTION

This chapter focuses on the hardware implementation of the interleaved boost converter with 25 W power rating developed within this project. Following the calculation and simulation phase, the next logical phase included fabrication of a small-scale prototype to analyse the behaviour of the interleaved converter in practice. In this stage, the objective of developing the hardware setup was to test the capability of boosting voltage, sharing of current among different phases, switching performance, and stability of the circuitry.

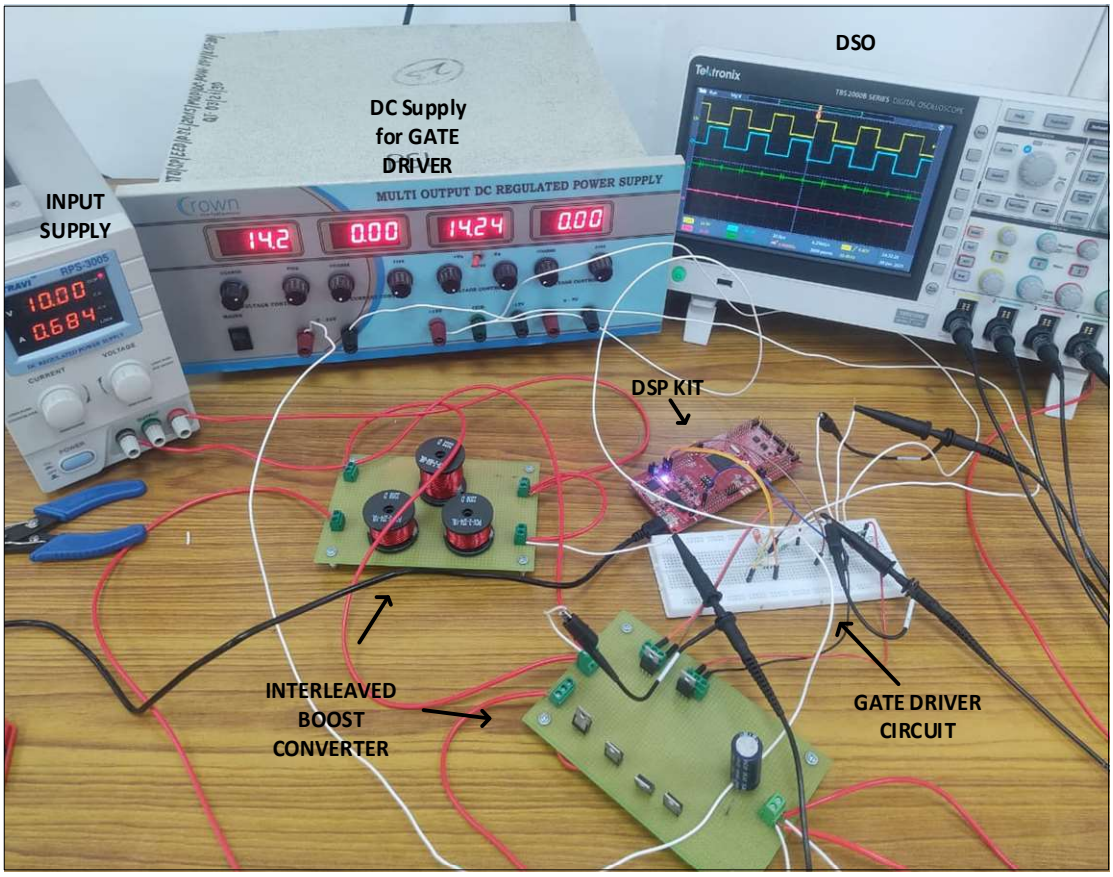

Fig: 5.1 Hardware Prototype (50W) (In Process)

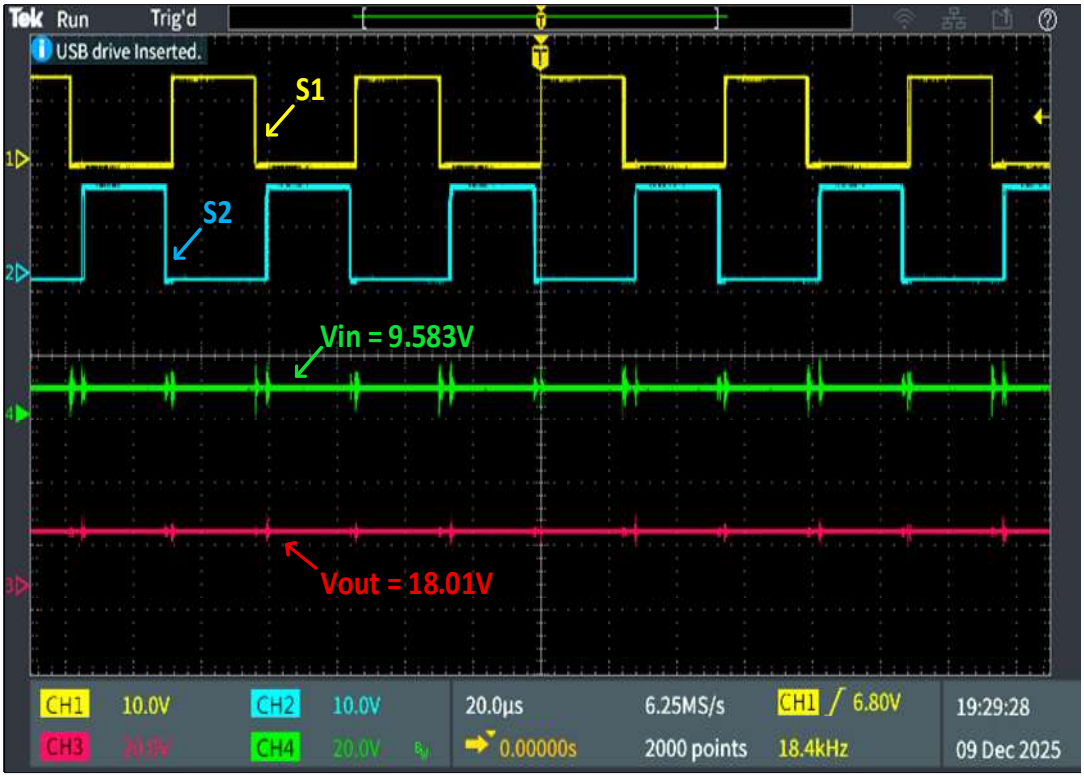

Fig5.2: Hardware Results with 45% Duty.

5.2 Conclusion

A working hardware prototype of the interleaved boost converter was also constructed and tested in the real-world environment. These tests have proved the validity of the theoretical calculations and simulations that support the voltage boosting capability of the designed structure. As is shown from the oscilloscope readings, the two gate signals S1 and S2 work in accordance with the theoretically predicted interleaving scheme with 45% duty cycle resulting in a stable voltage output of 18.01 V from an input of 9.583 V, which agrees very well with the theoretical conversion factor. The gate driver circuit along with the DSP control system operated effectively in the whole course of the experiments, proving thus the practical viability of the proposed approach.

CHAPTER 6

CONCLUSION AND FUTURE SCOPE

6.1 Conclusion

This paper outlined the design, simulation, and analysis of a two-stage AC-to-DC converter topology to be used in a two-wheeler electric vehicle charger with a rated power rating of 3 kW. The proposed topology comprised a pre-regulation stage and an isolation and regulation stage, where the former was used to preprocess a 230 V AC grid supply and provide an output of 48 V DC via a 400 V DC intermediary bus stage.

The pre-regulation topology employed an interleaved boost power factor correction converter with a dual-loop control mechanism consisting of a voltage regulation loop as the outer loop and the current regulation loop as the inner loop. The interleaved configuration of two parallel boost converters operating in a 180° phase difference greatly minimized the input current ripple and evenly distributed the heat generation within the switches. This, coupled with the use of the dual-loop control mechanism, resulted in the input current being almost in perfect synchronization with the sinusoidal reference wave form, producing a total harmonic distortion of less than 5% and a power factor close to unity at the input side of the system.

In the second stage, a full-bridge resonant LLC converter with output voltage regulation based on a PFM scheme was utilized. Using the resonant properties of the LLC resonant circuit, consisting of the series resonant inductance, resonant capacitor, and transformer's magnetizing inductance, ZVS switching of the primary side switches and ZCS operation of the secondary side diodes were achieved, minimizing the switching losses. By modulating the switching frequency close to the resonant frequency, the output voltage regulation at 48 V for two-wheeler battery charging was successfully achieved. Additionally, galvanic isolation provided by the high-frequency transformer helped ensure safety of users as per the EV charging regulations.

Overall, the integration of these two stages was thoroughly analyzed, showing that the use of 400 V DC bus makes the control of each stage independent. The simulation results prove adequate performance of the two-stage charger in terms of both steady-state and

dynamic responses. In conclusion, the proposed two-stage charger provides an optimal balance of a high power factor, minimum harmonic distortion, soft-switching operation, and output voltage regulation, which makes it applicable in EV charging applications for two-wheelers.

6.2 Future Scope

The simulations done here are representative of the system performance in general, however, hardware testing would present the real-world issues like efficiency losses, parasitic effects, and thermal effects which are hard to replicate in simulation, and as such a lab prototype of the system needs to be built as future work. Upon creation of hardware the control algorithms designed here could be ported onto a DSP or FPGA based digital platform, which would enable much more adaptive and responsive control than the current analog system. Only power from the AC grid could be fed to the battery in the current setup, whereas an extension to two-way power transfer would allow the system to feed power back into the grid, a subject that is becoming more and more prominent in the EV topic of V2G. A battery management system was not implemented as part of this project, thus a charging algorithm using constant current and constant voltage modes adapted to two-wheeler Li-ion battery would add significantly to the completion of this project. The 3kW rating was decided keeping two-wheelers in mind; however, the same control topology and logic could be easily adapted to four-wheeler charging at higher power levels with only modification in the transformers, etc. Lastly, since the LLC stage already incorporates a high frequency isolated transformer, the system may easily be used as a basis for a wireless power transfer system by using loosely coupled coils instead of the transformer, thus offering a convenient, cable-free solution.

REFERENCES

[1] J. Prakash and I. Sarkar, “Comparison of pfc converter topology for electric vehicle battery charger application,” in 2022 IEEE Students Conference on Engineering and Systems (SCES), 2022, pp. 1–6.

[2] Infineon, “PFC Boost Converter Design Guide 1200w design example,” https://www.infineon.com/assets/row/public/documents/24/42/infineon-applicationnote-pfcccmboostconverterdesignguide-applicationnotes-en.pdf

[3] Texas Instruments, *“An Interleaved PFC Preregulator for High-Power Converters,”* White Paper. [Online]. Available: https://www.ti.com/lit/wp/slua746/slua746.pdf

25 [4] Toshiba Electronic Devices & Storage Corporation, *“Resonant Circuits and Soft Switching (LLC Resonant Converter and Resonant Inverter),”* Application Note, Nov. 12, 2019.

[5] Infineon, “Design example resonant LLC converter operation and design,” https://www.infineon.com/assets/row/public/documents/24/42/infineon-design-example-resonant-llc-converter-operation-and-design-applicationnotes-en.pdf

[6] Infineon Technologies AG, *“LLC Design Guide: 3300 W Converter—Simplified Algorithm Based on FHA and Vector Method,”* Application Note. [Online]. Available: https://www.infineon.com/assets/row/public/documents/24/42/infineon-llc-design-guide-3300w-converter-applicationnotes-en.pdf

[7] S. Li, J. Deng and C. C. Mi, "Single-Stage Resonant Battery Charger With Inherent Power Factor Correction for Electric Vehicles," in *IEEE Transactions on Vehicular Technology*, vol. 62, no. 9, pp. 4336-4344, Nov. 2013

[8] I. -O. Lee and G. -W. Moon, "Analysis and Design of a Three-Level LLC Series Resonant Converter for High- and Wide-Input-Voltage Applications," in *IEEE Transactions on Power Electronics*, vol. 27, no. 6, pp. 2966-2979, June 2012

[9] Shreyas and M. Kumar, "Design and Analysis of LLC Resonant Converter for Electric Vehicle Battery Charging," *2023 IEEE 3rd International Conference on*

Sustainable Energy and Future Electric Transportation (SEFET), Bhubaneswar, India, 2023.

[10] S. Li, J. Deng and C. C. Mi, "Single-Stage Resonant Battery Charger With Inherent Power Factor Correction for Electric Vehicles," in *IEEE Transactions on Vehicular Technology*, vol. 62, no. 9, pp. 4336-4344, Nov. 2013

[11] Kim, J.H., Kim, C.E., Kim, J.K., Lee, J.B. and Moon, G.W., 2015. Analysis on load-adaptive phase-shift control for high efficiency full-bridge LLC resonant converter under light-load conditions. *IEEE Transactions on Power Electronics*, *31*(7), pp.4942-4955.

[12] Yeon, Cheol-O., Jong-Woo Kim, Moo-Hyun Park, Il-Oun Lee, and Gun-Woo Moon. "Improving the light-load regulation capability of LLC series resonant converter using impedance analysis." *IEEE Transactions on Power Electronics* 32, no. 9 (2016): 7056-7067.

[13] F. Yang, X. Ruan, Y. Yang and Z. Ye, "Interleaved Critical Current Mode Boost PFC Converter With Coupled Inductor," in *IEEE Transactions on Power Electronics*, vol. 26, no. 9, pp. 2404-2413, Sept. 2011

[14] X. Xu, W. Liu and A. Q. Huang, "Two-Phase Interleaved Critical Mode PFC Boost Converter With Closed Loop Interleaving Strategy," in IEEE Transactions on Power Electronics, vol. 24, no. 12, pp. 3003-3013.

[15] L. Huber, Y. Jang and M. M. Jovanovic, "Performance Evaluation of Bridgeless PFC Boost Rectifiers," in *IEEE Transactions on Power Electronics*, vol. 23, no. 3, pp. 1381-1390, May 2008.

[16] H. Valipour, M. Mahdavi, M. Ordonez, P. F. Ksiazek and R. M. Khandekar, "Extended Range Bridgeless PFC Converter With High-Voltage DC Bus and Small Inductor," in *IEEE Transactions on Power Electronics*, vol. 36, no. 1, pp. 157-173, Jan. 2021.

[17] F. Musavi, W. Eberle and W. G. Dunford, "A high-performance single-phase AC-DC power factor corrected boost converter for plug in hybrid electric vehicle battery chargers," *2010 IEEE Energy Conversion Congress and Exposition*, Atlanta, GA, USA, 2010.

[18] S. Li, J. Deng and C. C. Mi, "Single-Stage Resonant Battery Charger With Inherent Power Factor Correction for Electric Vehicles," in *IEEE Transactions on Vehicular Technology*, vol. 62, no. 9, pp. 4336-4344, Nov. 2013

[19] M. F. Menke and S. L. Avila, "Multi-objective Genetic Algorithm Based Optimal Design Methodology for LLC Resonant Converter," *2022 14th Seminar on Power Electronics and Control (SEPOC)*, Santa Maria, Brazil, 2022, pp. 1-6

[20] Kim, Keon-Woo, et al. "Analysis on synchronous rectifier control to improve regulation capability of high-frequency LLC resonant converter." *IEEE Transactions on Power Electronics* 33.8 (2017): 7252-7259.

[21] Kim, Dong-Kwan, SangCheol Moon, Cheol-O. Yeon, and Gun-Woo Moon. "High-efficiency LLC resonant converter with high voltage gain using an auxiliary LC resonant circuit." *IEEE Transactions on Power Electronics* 31, no. 10 (2015): 6901-6909.

[22] Lee, Jae-Bum, Chong-Eun Kim, Jae-Kuk Kim, Jae-Hyun Kim, Sang-Cheol Moon, and Gun-Woo Moon. "A novel accurate primary-side control (PSC) method for half-bridge (HB) LLC converter." *IEEE Transactions on Power Electronics* 30, no. 4 (2014): 1797-1803.

[23] Pandey, Rahul, and Bhim Singh. "Resonant LLC converter for E-bike charger." In 2019 International Conference on Electrical, Electronics and Computer Engineering (UPCON), pp. 1-6. IEEE, 2019.